Title
Development of Human Lateral Prefrontal Sulcal Morphology and Its Relation to Reasoning Performance.

Journal
Journal of Neuroscience, 43(14)

Authors
Willbrand, Ethan
Ferrer, Emilio
Bunge, Silvia
et al.

Publication Date
2023-04-05

DOI
10.1523/JNEUROSCI.1745-22.2023

Peer reviewed

Behavioral/Cognitive

Development of Human Lateral Prefrontal Sulcal Morphology and Its Relation to Reasoning Performance

Ethan H. Willbrand,[1,2] Emilio Ferrer,[3,4] Silvia A. Bunge,[1,2*] and Kevin S. Weiner[1,2*]
[1]Department of Psychology, [2]Helen Wills Neuroscience Institute, University of California Berkeley, Berkeley, California 94720, [3]Department of Psychology, and [4]Center for Mind and Brain, University of California–Davis, Davis, California 95616

Previous findings show that the morphology of folds (sulci) of the human cerebral cortex flatten during postnatal development. However, previous studies did not consider the relationship between sulcal morphology and cognitive development in individual participants. Here, we fill this gap in knowledge by leveraging cross-sectional morphologic neuroimaging data in the lateral PFC (LPFC) from individual human participants (6-36 years old, males and females; *N* = 108; 3672 sulci), as well as longitudinal morphologic and behavioral data from a subset of child and adolescent participants scanned at two time points (6-18 years old; *N* = 44; 2992 sulci). Manually defining thousands of sulci revealed that LPFC sulcal morphology (depth, surface area, and gray matter thickness) differed between children (6-11 years old)/adolescents (11-18 years old) and young adults (22-36 years old) cross-sectionally, but only cortical thickness showed differences across childhood and adolescence and presented longitudinal changes during childhood and adolescence. Furthermore, a data-driven approach relating morphology and cognition identified that longitudinal changes in cortical thickness of four left-hemisphere LPFC sulci predicted longitudinal changes in reasoning performance, a higher-level cognitive ability that relies on LPFC. Contrary to previous findings, these results suggest that sulci may flatten either after this time frame or over a longer longitudinal period of time than previously presented. Crucially, these results also suggest that longitudinal changes in the cortex within specific LPFC sulci are behaviorally meaningful, providing targeted structures, and areas of the cortex, for future neuroimaging studies examining the development of cognitive abilities.

Key words: lateral PFC; morphometry; neuroanatomy; neurodevelopment; neuroimaging; reasoning

Significance Statement

Recent work has shown that individual differences in neuroanatomical structures (indentations, or sulci) within the lateral PFC are behaviorally meaningful during childhood and adolescence. Here, we describe how specific lateral PFC sulci develop at the level of individual participants for the first time: from both cross-sectional and longitudinal perspectives. Further, we show, also for the first time, that the longitudinal morphologic changes in these structures are behaviorally relevant. These findings lay the foundation for a future avenue to precisely study the development of the cortex and highlight the importance of studying the development of sulci in other cortical expanses and charting how these changes relate to the cognitive abilities those areas support at the level of individual participants.

Received Aug. 24, 2022; revised Jan. 25, 2023; accepted Feb. 1, 2023.

Author contributions: E.H.W., E.F., S.A.B., and K.S.W. designed research; E.H.W., S.A.B., and K.S.W. performed research; E.H.W., S.A.B., and K.S.W. analyzed data; E.H.W. wrote the first draft of the paper; E.H.W., E.F., S.A.B., and K.S.W. edited the paper; E.H.W., S.A.B., and K.S.W. wrote the paper; E.F. contributed unpublished reagents/analytic tools.

*S.A.B. and K.S.W. contributed equally to this work as shared senior authors.

This work was supported by National Institute of Child Health and Human Development R21HD100858 to K.S.W. and S.A.B., and National Science Foundation Career Award 2042251 to K.S.W. Funding for the original data collection and curation of the pediatric sample was provided by National Institute of Neurological Disorders and Stroke R01 NS057156 to S.A.B. and E.F., and National Science Foundation BCS1558585 to S.A.B. and Wendelken. Data for the young adult sample were provided by the Human Connectome Project, WU-Minn Consortium (Principal Investigators: David Van Essen and Kamil Ugurbil; National Institutes of Health Grant 1U54-MH-091657) funded by the 16 National Institutes of Health and Centers that support the National Institutes of Health Blueprint for Neuroscience Research and by the McDonnell Center for Systems Neuroscience at Washington University. We thank former members of the S.A.B. laboratory for assistance with data collection; the families who participated in the original study; and Willa Voorhies, Jewelia Yao, Ishana Raghuram, and Jacob Miller for assistance in defining the lateral PFC sulci and developing the code used for this project.

The authors declare no competing financial interests.

Correspondence should be addressed to Silvia A. Bunge at sbunge@berkeley.edu or Kevin S. Weiner at kweiner@berkeley.edu.

https://doi.org/10.1523/JNEUROSCI.1745-22.2023

Introduction

Over the past decades, progress has been made toward understanding how the anatomy of the cerebral cortex broadly changes during human development. For example, prior work has shown that cortical gray matter decreases while cortical white matter and surface area increase (Gogtay et al., 2004; Sowell et al., 2004; Lebel et al., 2008; Shaw et al., 2008; Brown et al., 2012; Amlien et al., 2016; Tamnes et al., 2017; de Faria et al., 2021; Norbom et al., 2021; Baum et al., 2022; Bethlehem et al., 2022; Fuhrmann et al., 2022). Nevertheless, a critical gap in knowledge remains: How do neuroanatomical structures within the cerebral cortex, especially those that are hominoid-specific, develop at the individual level?

To address this question, the present study focuses on the development of lateral PFC (LPFC), for several key reasons. First, LPFC is relatively enlarged in humans compared with other commonly studied nonhuman primates (Semendeferi et al., 2002; Donahue et al., 2018). Second and third, LPFC is one of the slowest maturing cortical regions (Gogtay et al., 2004; Tamnes et al., 2013; Chini and Hanganu-Opatz, 2021) and plays a central role in many later-developing cognitive abilities, such as reasoning (Luria, 1966; Milner and Petrides, 1984; Krawczyk, 2012; Stuss and Knight, 2013). Fourth, LPFC contains indentations, or sulci, that are either hominoid-specific or human-specific (Amiez and Petrides, 2007; Petrides, 2019; Miller et al., 2021a, 2021b; Voorhies et al., 2021; Hathaway et al., 2022; Willbrand et al., 2022b; Yao et al., 2022). Importantly, the morphology (Voorhies et al., 2021; Yao et al., 2022) and the presence or absence of these variable LPFC sulci (Willbrand et al., 2022b) are related to cognitive abilities. Thus, human LPFC is a heterogeneous entity with sulci that show striking individual differences in morphology that are related to individual differences in cognition, a relationship that necessitates studying LPFC sulcal development at the individual level.

Indeed, analyses at the lobular or group level would likely fail to accurately capture the developmental trajectories of these cortical structures because such analyses obscure this individual variability as previously shown (Miller et al., 2021a, 2021b; Voorhies et al., 2021). For example, one study showed that the cortex "flattens" at the lobular level across ages 11-17, exhibiting increases in sulcal width and decreases in sulcal depth, thickness, and local gyrification, especially in the frontal lobe (Alemán-Gómez et al., 2013). Nevertheless, while these results have helped guide the field, it is presently unknown whether these findings extend to analyses conducted at a more granular level, such as the development of LPFC sulci at the individual level. Accordingly, age-related changes in the majority of these LPFC sulci and the behavioral relevance of such changes are largely unknown.

Given the limitations of "large N," group-level analyses for studying sulcal morphology (Miller et al., 2021a,b), here, we took a "deep imaging" approach (Gratton et al., 2022) to study age-related changes in sulcal morphology and brain-behavior relationships by focusing on a large sampling of individual sulci within individual participants. To this end, we first leveraged individual LPFC sulcal data (3672 sulcal definitions) from 108 participants (6-36 years old) from previous work in pediatric (Voorhies et al., 2021; Willbrand et al., 2022b; Yao et al., 2022) and young adult samples (Miller et al., 2021b) to address whether the morphology of these sulci differs cross-sectionally during this time frame. We then defined 2992 sulci (1496 per time point) in a subset of the pediatric participants scanned at two time points ($N = 44$) to determine whether LPFC sulcal morphology changes longitudinally, across an average time frame of 1.6 years. Finally, we tested whether longitudinal changes in LPFC sulcal morphology predicted longitudinal changes in a reasoning task that relies on LPFC (Milner and Petrides, 1984; Christoff et al., 2001; Crone et al., 2009; Vendetti and Bunge, 2014).

Table 1. Gender and age demographics of the three age groups[a]

Age group	*n* (% F)	Age [(yr) ± SD]	Age range (yr)
Children	36 (47.2)	8.9 ± 1.59	6.41-11.53
Adolescents	36 (36.1)	15.21 ± 2.15	11.66-18.86
Young adults	36 (47.2)	28.97 ± 3.78	22-36

[a]Additional demographic information is included in Extended Data Tables 1-1 and 1-2.

Materials and Methods

Participants

Children and adolescents

General details. The present study leveraged previously published data from the longitudinal Neurodevelopment of Reasoning Ability dataset (Wendelken et al., 2011, 2016, 2017; Ferrer et al., 2013; Voorhies et al., 2021; Willbrand et al., 2022b; Yao et al., 2022). All participants were screened for neurologic impairments, psychiatric illness, history of learning disability, and developmental delay. Participants and their parents gave their informed assent and/or consent to participate in the study, which was approved by the Committee for the Protection of Human Participants at the University of California, Berkeley.

Cross-sectional sample. Seventy-two typically developing individuals (30 females and 42 males, based on parent-reported gender identity) between the ages of 6 and 18 (average age ± SD: 12.06 ± 3.69 years) were randomly selected from the dataset. The descriptive statistics represent the ages of the selected participants at the time of the selected scan. These participants were the same as those used in previous studies examining the relationship between the morphology of LPFC sulci and behavior (Voorhies et al., 2021; Willbrand et al., 2022b; Yao et al., 2022). For cross-sectional analyses, we divided this pediatric sample along the median age (11.6 years) to establish two equally sized age groups (children: mean age ± SD: 8.90 ± 1.59 years, 6.41-11.53 years old; adolescents: mean age ± SD: 15.21 ± 2.15 years, 11.66-18.86 years old) to the young adult sample (Table 1). Additional demographic and socioeconomic data are included in Extended Data Tables 1-1.

Longitudinal sample. Of the 72 participants comprising the children and adolescent sample, 49 (19 females and 30 males) were scanned at two separate time points (average age at baseline ± SD: 10.82 ± 3.44 years, 6.25-17.65; average age at follow-up ± SD: 12.37 ± 3.58 years, 7.57-19.32 years; average number of years between scans ± SD: 1.55 ± 0.44 years). These initial 49 participants were tentatively selected for longitudinal morphologic analyses; however, because of subsequent selection criteria (see below), the morphologic analyses were conducted on 44 participants (females = 18, males = 26; average age at baseline ± SD: 11.1 ± 3.47 years; average number of years at follow-up ± SD: 12.66 ± 3.61 years; average number of years between scans ± SD: 1.56 ± 0.46 years).

Young adults

We analyzed young adult structural MRI data from the freely available Human Connectome Project database (HCP; https://www.humanconnectome.org/study/hcp-young-adult) (Van Essen et al., 2012). This cross-sectional dataset consisted of 36 randomly selected HCP participants (17 females and 19 males) whose ages were between 22 and 36 (average age ± SD: 28.97 ± 3.78 years). For additional demographic and socioeconomic information, see Extended Data Tables 1-2. These participants were the same as those used in a previous study examining the anatomic and functional features of LPFC sulci (Miller et al., 2021b). These data were previously acquired using protocols approved by the Washington University Institutional Review Board.

Behavioral data

Children and adolescents

The majority of participants from the children and adolescent sample had scores for the WISC-IV matrix reasoning task (Wechsler, 1949), a widely used, gold-standard measure of abstract, nonverbal reasoning (Ferrer et al., 2013; Wendelken et al., 2016) that relies on LPFC (for review, see Holyoak and Monti, 2021). Matrix reasoning is an untimed subtest of the WISC-IV in which participants are shown colored matrices with one missing quadrant. The participant is asked to complete the matrix by selecting the appropriate quadrant from an array of options. To maximize our sample size, we focused on the longitudinal relationship between sulcal morphology and raw matrix reasoning scores. The longitudinal morphologic-behavioral analyses were conducted with the 43 participants from the longitudinal subset of the pediatric sample (female = 18; male = 25) who completed the WISC-IV matrix reasoning task at both time points (average age at baseline ± SD: 11.1 ± 3.43 years; average number of years at follow-up ± SD: 12.66 ± 3.57 years; average number of years between scans ± SD: 1.56 ± 0.46 years).

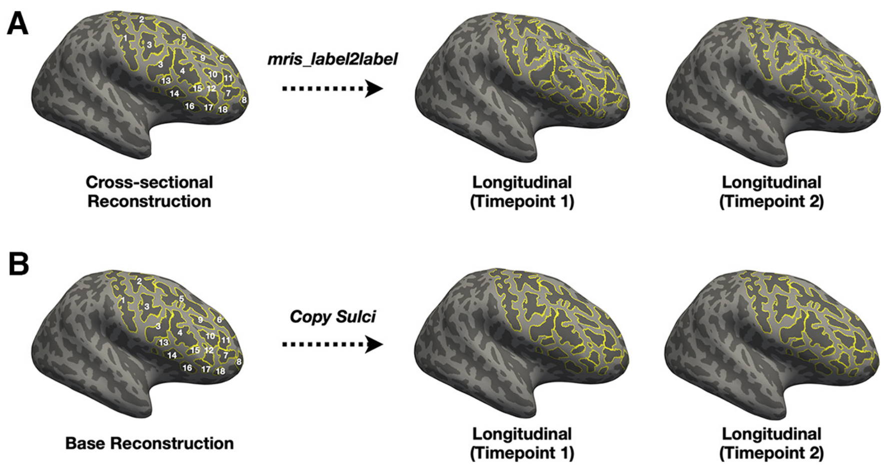

Figure 1. Methodological pipeline for defining individual LPFC sulci longitudinally. ***A***, Cross-sectional (left) and longitudinal (right) inflated cortical surfaces (sulci: dark gray; gyri: light gray) for an example participant. LPFC sulci are outlined in yellow, and the numbers identifying each sulcus correspond with those in Table 2. Projecting sulcal labels from the cross-sectional surfaces (see Materials and Methods) to the longitudinal surfaces with *mris_label2label* does not provide accurate sulcal definitions. ***B***. The same format as in ***A***, but with the base template (left) inflated cortical surface for this example participant. For the longitudinal analyses, LPFC sulci were manually redefined on the base surfaces (see Materials and Methods) since projecting these labels from the base template to the longitudinal surfaces provides highly accurate individual labels on the longitudinal surfaces, in contrast to ***A***. This process ensures that each sulcus is indeed the same structure at both time points.

Imaging data acquisition

Children and adolescents

High-resolution T1-weighted MPRAGE anatomic scans (TR = 2300 ms, TE = 2.98 ms, 1 mm isotropic voxels) were acquired using the Siemens 3T Trio fMRI scanner at the University of California Berkeley Brain Imaging Center. For participants included in the longitudinal analyses, two anatomic scans were collected across an average delay of 1.56 ± 0.46 years (0.87-3.28 years) between time points.

Young adults

Anatomical T1-weighted MPRAGE anatomic scans (0.8 mm isotropic voxel resolution) were obtained in native space from the HCP database, along with outputs from the HCP modified FreeSurfer pipeline (Dale et al., 1999; Fischl et al., 1999a; Glasser et al., 2013). Additional details on image acquisition parameters and image processing can be found in Glasser et al. (2013).

Morphologic analyses

Cross-sectional cortical surface reconstruction pipeline

Each T1-weighted image was visually inspected for scanner artifacts. Afterward, reconstructions of the cortical surfaces were generated for each participant from their T1 scans using a standard FreeSurfer pipeline (version 6.0.0; https://surfer.nmr.mgh.harvard.edu/) (Dale et al., 1999; Fischl et al., 1999a, 1999b). Cortical reconstructions were created from the resulting boundary made by segmenting the gray and white matter in each anatomic volume with FreeSurfer's automated segmentation tools (Dale et al., 1999). Each reconstruction was inspected for segmentation errors, which were then manually corrected when necessary. Subsequent sulcal labeling and extraction of anatomic metrics were calculated from individual participants' cortical surface reconstructions.

Longitudinal cortical surface reconstruction pipeline

The FreeSurfer longitudinal Stream (version 6.0.0; https://surfer.nmr.mgh.harvard.edu/fswiki/LongitudinalProcessing) (Reuter et al., 2012) was leveraged to create accurate and unbiased cortical reconstructions of the two independent scans that were obtained for each individual participant for whom we had scans at two time points. Here, we briefly describe this longitudinal processing pipeline (for additional details, see Reuter et al., 2010, 2012; Reuter and Fischl, 2011). First, the two T1-weighted images for each participant are processed independently using the standard FreeSurfer pipeline described previously (Dale et al., 1999; Fischl et al., 1999a, 1999b). Second, an unbiased within-subject template space and image (base template) is created from these two independent images using robust, inverse consistent registration (Reuter et al., 2010; Reuter and Fischl, 2011). Third, after the creation of this base template, these independent, cross-sectional images are processed again; however, several processing steps (e.g., skull stripping, Talairach transforms, atlas registration as well as spherical surface maps and parcellations) are initialized with common information from the within-subject template. This procedure significantly increases reliability and statistical power, as well as the robustness and sensitivity of the overall longitudinal analysis (Reuter et al., 2010, 2012). In addition, new probabilistic methods were applied to further reduce the variability of results across time points.

Each reconstruction was also inspected for major topological errors between the first two steps. Participants were excluded if one of their reconstructions was of insufficient quality. In total, 5 participants (females = 1, males = 4; average age at baseline ± SD: 8.4 ± 2.18 years; average age at follow-up ± SD: 9.82 ± 2.22 years; average number of years between scans ± SD: 1.43 ± 0.15 years) were excluded because of having a poor reconstruction at one time point, resulting in the final sample of 44 participants for longitudinal morphologic analyses.

General procedure for manual labeling of LPFC sulci

The majority of the sulci described here were originally defined in these two samples for previous work studying the relationship between LPFC sulci and anatomic, functional, and behavioral features (see Miller et al., 2021a, 2021b; Voorhies et al., 2021; Willbrand et al., 2022b; Yao et al., 2022). Sulcal labels in the LPFC were based on the most recent parcellation proposed by Petrides (2019; see also Sprung-Much and Petrides, 2018, 2020).

LPFC sulci were manually defined in each hemisphere and each participant on both the pial and inflated surfaces (for further details, see Miller et al., 2021b; Voorhies et al., 2021). An example hemisphere is shown in Figure 1*A*, left (for a summary of the 18 identifiable LPFC sulci, see Table 2). We first defined the three larger sulci that serve as the posterior boundary of LPFC, namely, the (1) central sulcus (cs), as well as (2) the superior (sprs) and (3) inferior (iprs) components of the precentral sulcus. We then defined the large sulcus running longitudinally across LPFC: the inferior frontal sulcus (ifs). We then defined eight sulci anterior to the prcs and superior to the ifs: (1) the anterior (sfs-a) and (2) posterior (sfs-p) components of the superior frontal sulcus (sfs), (3) the vertical (imfs-v) and (4) horizontal (imfs-h) components of the intermediate fronto-marginal sulcus (imfs), (5) the anterior (pmfs-a), (6) intermediate (pmfs-i), and (7) posterior (pmfs-p) components of the posterior middle frontal sulcus (pmfs), and (8) the para-intermediate

Table 2. Sulcal definitions of the 18 LPFC sulci explored in the present study[a]

No.	Abbreviation	Name
1	cs	central sulcus
2	sprs	superior precentral sulcus
3	iprs	inferior precentral sulcus
4	ifs	inferior frontal sulcus
5	sfs-p	superior frontal sulcus, posterior
6	sfs-a	superior frontal sulcus, anterior
7	imfs-h	intermediate frontal sulcus, horizontal
8	imfs-v	intermediate frontal sulcus, vertical
9	pmfs-p	posterior middle frontal sulcus, posterior
10	pmfs-i	posterior middle frontal sulcus, intermediate
11	pmfs-a	posterior middle frontal sulcus, anterior
12	pimfs[b]	paraintermediate frontal sulcus
13	ds	diagonal sulcus
14	aalf	ascending ramus of the lateral fissure
15	ts	triangular sulcus
16	half	horizontal ramus of the lateral fissure
17	prts	pretriangular sulcus
18	lfms	lateral frontomarginal sulcus

[a]Numbers correspond to sulci in Figures 1 and 2. Sulcal abbreviations and the full name are included.
[b]The pimfs can have 0, 1, or 2 components (dorsal and ventral) (Voorhies et al., 2021; Yao et al., 2022; Willbrand et al., 2022b). The pimfs is not included in our analyses because of this variability.

frontal sulcus (pimfs). These 12 sulci have previously been identified in children and adolescents (Voorhies et al., 2021; Willbrand et al., 2022b; Yao et al., 2022), as well as in young adults (Miller et al., 2021b). Finally, we defined the six sulci inferior to the ifs: the diagonal sulcus (ds), the triangular sulcus (ts), the pretriangular sulcus (prts), the lateral marginal frontal sulcus (lfms), the ascending ramus of the lateral fissure (aalf), and the horizontal ramus of the lateral fissure (half). These six sulci were previously identified in children and adolescents by Yao et al. (2022), and in young adults for the present study. One of these 18 sulci, *pimfs*, showed a high degree of variability, with individuals exhibiting 2, 1, or 0 branches in a given hemisphere (Voorhies et al., 2021; Willbrand et al., 2022b); as a result, this sulcus was not included in our developmental morphologic analyses. All in all, the present study considered 17 of the 18 total LPFC sulci that were reliably identified across participants and hemispheres.

As in our previous work, each LPFC sulcus was manually defined within each individual hemisphere on the FreeSurfer *inflated* mesh with tools in *tksurfer*, which enables accurate definition of individual sulci within *in vivo* MRI data (Weiner et al., 2014, 2018; Miller et al., 2021a, 2021b; Voorhies et al., 2021). Specifically, the *curvature* metric in FreeSurfer distinguished the boundaries between sulcal and gyral components, which can be explored in greater detail on their website (https://surfer.nmr.mgh.harvard.edu). Briefly, on this scale, curvature values correspond to the "sharpness" of the curve of a given vertex. The sharper a curve, the larger the value. Gyri are defined as negative values, which correspond to curves pointing down. Sulcal vertices are positive values, which correspond to curves pointing up. We used the *binary* curvature option set by FreeSurfer to distinguish all gyral and sulcal vertices on each surface. This option binarizes all vertices based on the midpoint (i.e., zero) such that all sulcal vertices (i.e., all positive) are dark gray and all gyral vertices are light gray (i.e., all negative).

Manual lines were drawn on the *inflated* cortical surface to define sulci based on the proposal by Petrides (2019), and guided by the *pial* and *smoothwm* surfaces of each individual. Since the precise start or end point of a sulcus can be difficult to determine on one surface (Borne et al., 2020), using the *inflated*, *pial*, and *smoothwm* surfaces of each individual allows us to form a consensus across surfaces to clearly determine each sulcal boundary. The sulcal labels were generated using a two-tiered procedure. The location and definition of each label were first confirmed through a qualitative inter-rater reliability process (E.H.W., W.I.V., J.K.Y., I.R., and J.A.M.) and then finalized by a neuroanatomist (K.S.W.). All anatomic labels for a given hemisphere were fully defined before any morphologic analyses of the sulcal labels were quantified.

Modified procedure to manually label LPFC sulci longitudinally

After obtaining the two longitudinal reconstructions for the 44 participants, we first manually redefined the LPFC sulci on the *base* template of each participant (Fig. 1*B*, left, for an example hemisphere). This first step was performed since defining sulci on the base template surface and copying these labels to the longitudinal surfaces provides far more accurate sulcal definitions compared with using the *mris_label2label* function to convert labels from the cross-sectional surface to the longitudinal surfaces (Fig. 1). Once all sulci were defined on the base template, the sulcal labels were copied to the two time points to extract sulcal morphologic features at each time point. When necessary, minor corrections were made to sulcal labels at each time point before extracting morphologic features. The sulcal definitions and corrections in this step were completed by E.H.W. and K.S.W.

Extracting morphologic features from sulcal labels

After defining LPFC sulci in FreeSurfer, we extracted the following morphologic metrics from each sulcal label file: sulcal depth (mm), surface area (mm^2), and cortical thickness (mm). We selected sulcal depth and surface area as these metrics are prominent features of sulci (Sanides, 1964; Chi et al., 1977; Welker, 1990; Armstrong et al., 1995; Weiner et al., 2014, 2018; Lopez-Persem et al., 2019; Madan, 2019; Petrides, 2019; Weiner, 2019; Miller et al., 2020, 2021a, 2021b; Natu et al., 2021; Voorhies et al., 2021; Li et al., 2022; Willbrand et al., 2022a, 2022b; Yao et al., 2022). We further selected cortical thickness since the longitudinal development of cortical sulcal thickness was previously analyzed at the lobular level (Alemán-Gómez et al., 2013).

Raw depth values (in mm) were calculated using a custom-modified version of a recently developed algorithm built on the FreeSurfer pipeline (Madan, 2019). Briefly, depth was calculated as the distance between the sulcal fundus and the smoothed outer pial surface (Madan, 2019). Mean thickness and surface area values were extracted from each sulcus using the built-in *mris_anatomic_stats* function in FreeSurfer (Fischl and Dale, 2000). To account for differences in brain size across individuals and hemispheres, as in our prior work (Miller et al., 2020; Voorhies et al., 2021; Willbrand et al., 2022a, 2022b; Yao et al., 2022), we also calculated normalized values of thickness and depth to the thickest and deepest points, which are in the insula across species and hemispheres (Miller et al., 2020; Voorhies et al., 2021; Willbrand et al., 2022a; Yao et al., 2022). Surface area was normalized to hemispheric surface area in accordance with prior work (Zhou et al., 2014; Willbrand et al., 2022b).

Although prior work examining sulcal morphology studied sulcal width (for examples, see Alemán-Gómez et al., 2013; Cao et al., 2017; Jin et al., 2018; Carmona et al., 2019), we found that the current toolbox that can extract this information from individual sulcal labels in FreeSurfer (Madan, 2019) failed to obtain the width of many of the smaller sulci in LPFC. Thus, we were not able to examine this feature in the present study. With improved methodology, future work should seek to examine how the width of all LPFC sulci changes during development. In addition, while the study forming the basis of the present project (Alemán-Gómez et al., 2013) included lobular local gyrification index (lGI) values, we did not include this metric. The calculation of lGI in FreeSurfer is not done specific to a particular sulcus, but rather based on the folding of a cortical area, and fine-grained, vertex-level, values are also dependent on the specific parameters used (see Schaer et al., 2008, 2012). Therefore, we did not include lGI because it is more well suited for regional, lobular, or cortex-level analyses (as in Alemán-Gómez et al., 2013), not analyses at the level of individual sulci.

Classifying LPFC sulci based on morphology

Overview. We used an unsupervised, data-driven approach to group LPFC sulci based on their morphology: namely, a combination of *k*-means clustering and multidimensional scaling using the three morphologic features of sulci analyzed in this study (sulcal depth, surface area, and cortical thickness). These analyses were run on scaled morphologic data, separately in each hemisphere. Importantly, these analyses were conducted in a manner that was blind to age group (children, adolescents, and young adults) and sulcal type (primary, secondary, and tertiary) (for further details, see Miller et al., 2021a, 2021b; Voorhies et al., 2021; Yao et al., 2022).

Statistics. All morphologic analyses were implemented in R (version 4.1.2; http://www.r-project.org). Rather than choosing the number of clusters (k) ourselves or with a single index, we quantitatively determined the optimal number of clusters using the *NbClust* function (from the *NbClust* R package; https://www.rdocumentation.org/packages/NbClust/versions/3.0.1/topics/NbClust). Briefly, this function leverages 30 indices to propose the best number of clusters for the data based on the majority rule (for additional details, see Charrad et al., 2014). In both hemispheres, the majority of indices determined that three was the optimal number of clusters to describe the data. k-means clustering was then implemented using the *kmeans* function (from the *stats* R package; https://www.rdocumentation.org/packages/stats/versions/3.6.2) with the optimal number of clusters ($k = 3$) suggested by the *NbClust* function. Next, given the multidimensionality of the dataset (dimensions = 4), we ran classic (metric) multidimensional scaling with the *dist* and *cmdscale* R functions (from the *stats* R package) to visualize the (dis)similarity of the data and clusters in a lower-dimensional space (dimensions = 2). Cluster plots were then generated (using the *ggscatter* function from the *ggpubr* R package; https://rpkgs.datanovia.com/ggpubr/) to visualize the results. Finally, for subsequent morphologic analyses, the assignment of each LPFC sulcus to a cluster was determined by the majority rule, that is, it was based on what cluster the majority of participants fell into for each sulcus. Although our initial clustering was run blind to age, to confirm the robustness of the clusters for our developmental analyses, we also tested whether they differed in each age group separately.

Comparing the morphology of LPFC sulci between age groups cross-sectionally

Overview. To compare the depth, thickness, and surface area of LPFC sulci between the three established age groups (children, adolescents, and young adults; Table 1), we used mixed-model ANOVAs. For each ANOVA, hemisphere (left, right) and sulcal cluster (three clusters) were used as within-participant factors, while age group (children, adolescent, young adult) and gender (male, female) were implemented as between-participant factors. Hemisphere and gender were included because of prior research showing hemispheric differences in sulcal development (Chi et al., 1977) and mixed results regarding gender differences in sulcal development (Welker, 1990; Gottfredson, 1997). To determine whether the presence/absence of age group differences between the children and adolescent groups was limited to the categorical partitioning, we subsequently tested for a linear relationship between the morphologic metrics and age using the combined children and adolescent sample ($N = 72$; Table 1). We built linear mixed-effects models for each cluster. Model predictors included age and hemisphere, as well as their interaction terms. Hemisphere was nested within participant. ANOVAs and linear mixed-effects were repeated with the normalized metrics as the dependent variables.

Statistics. All ANOVAs were performed with the *aov_ez* function (from the *afex* R package; https://afex.singmann.science/). The Greenhouse–Geisser sphericity correction method was applied for all ANOVAs, which adjusted the degrees of freedom. Effect sizes are reported with the generalized η-squared (η^2G) metric. *Post hoc* pairwise comparisons on any significant main effects or interactions were performed with Tukey's method using the *emmeans* function (from the *emmeans* R package; https://github.com/rvlenth/emmeans). Linear mixed-effects were implemented with the *lme* function from the *nlme* R package (https://svn.r-project.org/R-packages/trunk/nlme/). Given the large number of tests performed, $p < 0.05$ was considered significant for any main effect or interaction after controlling for multiple comparisons (via the false discovery rate [FDR]).

Assessing whether LPFC sulcal morphology changes longitudinally

Overview and statistics. Considering the complexity of our longitudinal sulcal data (2 time points, 17 LPFC sulci, 2 hemispheres, 3 clusters), for the present study, we averaged values across the sulci within each cluster (Fig. 2*B*) to create three "cluster averages" for each morphologic feature in each hemisphere for each participant at each time point. This grouping was based on the cross-sectional clusters and conducted before running longitudinal analyses. We primarily tested for longitudinal changes in cortical thickness, which was the only feature to show differences between children and adolescents in the cross-sectional analyses (see Results). Linear growth curve models were run to examine changes in cortical thickness from Time point 1 to Time point 2 for each cluster in each hemisphere. We also regressed cortical thickness on baseline age to test whether this factor influenced the level (the thickness at Time point 1) and slope (the change from Time point 1 to Time point 2) for each cluster. We also tested sulcal depth given its behavioral and developmental relevance (Alemán-Gómez et al., 2013; Voorhies et al., 2021; Yao et al., 2022). Gender was not included in the models since it was not related to either LPFC morphologic metric cross-sectionally (see Results) or changes in morphology for any cluster (p values > 0.41). Linear growth curves were implemented with the *SEM* function (from the *lavaan* R package; https://lavaan.ugent.be/).

Longitudinal behavioral analyses

Model selection

Overview. We assessed whether individual differences in changes in sulcal cortical thickness (ΔCT) predicted variability in changes in matrix reasoning performance (ΔMR). As in prior work (Voorhies et al., 2021; Yao et al., 2022), we leveraged a least absolute shrinkage and selection operator (LASSO) regression, separately in each hemisphere, to select which of the LPFC sulci examined in this study, if any, showed ΔCT associated with ΔMR.

A LASSO regression is well suited to address our question since it facilitates the model selection process and increases the generalizability of a model by providing a sparse solution that reduces coefficient values and decreases variance in the model without increasing bias (Heinze et al., 2018). Further, regularization is recommended in cases where there are many predictors ($X > 10$), as in this study, because this technique guards against overfitting and increases the likelihood that a model will generalize to other datasets. A LASSO performs L1 regularization by applying a penalty, or shrinking parameter (α), to the absolute magnitude of the coefficients. In this manner, low coefficients are set to zero and eliminated from the model. Therefore, LASSO affords data-driven variable selection that results in simplified models containing only the most predictive features, in this case, sulci predicting reasoning performance. Not only does this methodology improve model interpretability and prediction accuracy, but it also protects against overfitting, thus improving generalizability (Heinze et al., 2018; Ghojogh and Crowley, 2019).

Statistics. We used cross-validation to optimize the values for α as part of the model selection process with the *GridSearchCV* function from the *SciKit-learn* package in Python (https://scikit-learn.org/stable/modules/generated/sklearn.model_selection.GridSearchCV.html). *GridSearchCV* performs an exhaustive search across a range of specified α values. According to standard practices (Heinze et al., 2018), we then selected the α value (and corresponding model) that minimized the cross-validated mean-squared error (MSE_{cv}). All regression models were implemented with the *SciKit-learn* package in Python (Pedregosa et al., 2011).

Model comparisons

Overview. To specifically characterize the relationship between ΔCT and ΔMR, we compared the model determined by the LASSO regression to two alternative nested models. All models examined only left hemisphere sulci since the LASSO regressions only identified sulci in the left hemisphere as behaviorally relevant (left hemisphere: $\alpha = 0.07$; see Fig. 5*A*). The model did not select any right-hemisphere LPFC sulci at the α values with the lowest MSE_{cv} ($\alpha = 0.5$, $MSE_{cv} = 27.12$). As reasoning performance improves over childhood (Ferrer et al., 2013; Wendelken et al., 2016, 2017), and ΔMR was correlated with baseline age ($r = -0.43$, $p = 0.004$), we included age at baseline as an additional predictor of ΔMR in the three models. We did not include another potentially relevant time-related variable (Δtime) in these models as it did not relate to ΔMR ($p = 0.78$).

To confirm the results of our selection, we first constructed a simplified linear model with the four left-hemisphere LPFC sulci that were

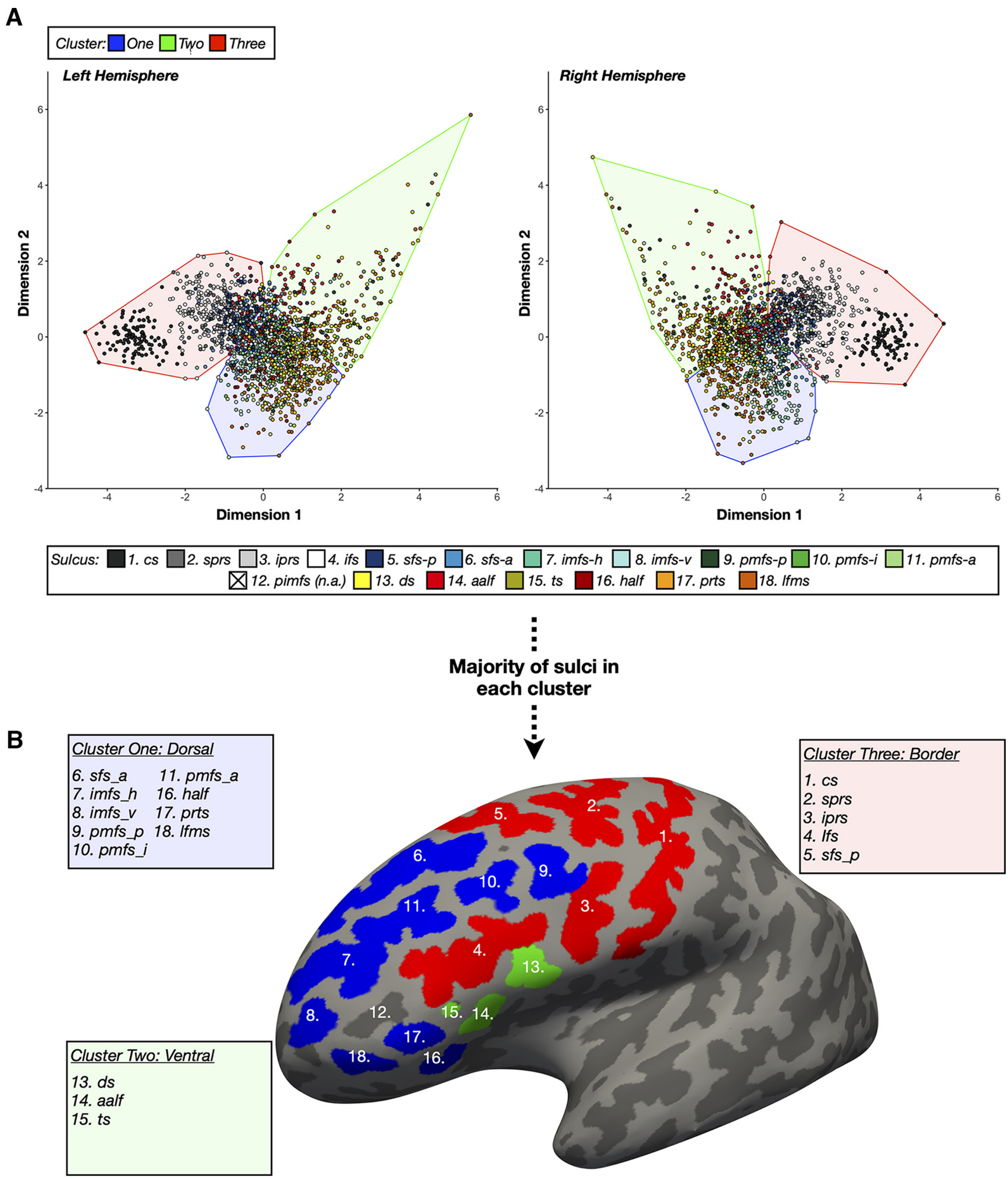

Figure 2. A data-driven approach clusters LPFC sulci into three groups based on morphology. ***A***, Cluster plots visualizing the results of the *k*-means clustering and multidimensional scaling analysis performed in each hemisphere (left: left hemisphere; right: right hemisphere). Individual dots represent individual sulci for all 108 participants and are colored by sulcus (see legend). The optimal number of clusters that described the LPFC sulci based on morphology was three: one (blue), two (green), and three (red). The sulci in each of the three clusters are encircled by a colored ellipse (see legend at top). ***B***, Example left hemisphere inflated cortical surface (sulci: dark gray; gyri: light gray). Colors represent the cluster in which each LPFC sulcus was quantitatively determined based on our data-driven approach (as in ***A***). The numbers identifying each LPFC sulcus on the cortical surface correspond with those in Table 2. Each box contains a list of the abbreviated names of the sulci in each cluster. Generally, Cluster 1 contained dorsal LPFC sulci, whereas Cluster 2 contained ventral LPFC sulci. Cluster 3 contained the sulci that border Clusters 1 and 2 posteriorly or in-between. Clustering results in each age group are shown in Figure 3.

selected by the LASSO regression as the strongest predictors of ΔMR. We refer to this simplified model as the LASSO-derived model (Eq. 1).

$$\hat{y}_i = \beta_0 + \beta_1 \text{Baseline Age} + \beta_2 \text{pmfs-a} + \beta_3 \text{aalf} + \beta_4 \text{prts} + \beta_5 \text{lfms} + \in I \quad (1)$$

We then compared the fit of the LASSO-derived model with a full model that included the ΔCT of all LPFC sulci within the left hemisphere, as well as baseline age (Eq. 2).

$$\hat{y}_i = \beta_0 + \beta_1 \text{Baseline Age} + \beta_2 x_2 \ldots + \beta_{18} x_{18} + \in I \quad (2)$$

In the nested full model, x_2–x_{18} represents the change in ΔCT of each of the 17 LPFC sulci in the left hemisphere included in this study, and β_2–β_{18} represents the associated coefficients.

Finally, we compared our LASSO-derived model, which included both baseline age and the ΔCT of the selected sulci (Eq. 1), to a model with baseline age as the sole predictor (Eq. 3). This nested comparison allowed us to discern whether the LPFC sulci in our selected model explained variance in ΔMR not captured by baseline age alone.

$$\hat{y}_i = \beta_0 + \beta_1 \text{Baseline Age} + \in I \quad (3)$$

Statistics. All linear models were fitted with a LOOCV procedure using the *SciKit-learn* package in Python (Pedregosa et al., 2011). Since these are nested models (wherein the largest model includes all elements in the smaller models), the model with the best fit was determined as the cross-validated model with the lowest MSE_{cv} and the highest R^2_{cv} values.

Data availability

The processed data required to perform all statistical analyses and to reproduce all figures for this project will be freely available with the publication of the paper on GitHub (https://github.com/cnl-berkeley/stable_projects). Requests for further information or raw data should be directed to the corresponding authors: K.S.W. (kweiner@berkeley.edu) and S.A.B. (sbunge@berkeley.edu).

Results

A data-driven approach produced three clusters of LPFC sulci based on a combination of morphologic features

Classic and modern studies acknowledge primary, secondary, and tertiary sulci based on several criteria, such as the time point in which sulci emerge in gestation, depth, surface area, and variability in the presence or absence of sulci. Nevertheless, perhaps unsurprisingly, neuroanatomists have continued to argue about which sulci are lumped into each group for decades. To circumvent these arguments, we implemented a data-driven approach that used a combination of *k*-means clustering and multidimensional scaling to test whether the 17 LPFC sulci in the present study could be grouped based on the three morphologic features extracted in the present study (see Materials and Methods; sulcal depth, surface area, and cortical thickness).

This analysis revealed that, regardless of qualitative definitions of primary, secondary, and tertiary sulci, LPFC sulci could be quantitatively grouped into three clusters (Fig. 2*A*, 3). Cluster 1 consisted primarily of dorsal PFC sulci (sfs-a, imfs-h, imfs-v, pmfs-p, pmfs-i, pmfs-a, lfms, prts, and half), Cluster 2 primarily of ventral PFC sulci (ts, ds, and aalf), and Cluster 3 primarily of PFC sulci bordering Cluster 1 and Cluster 2, either in-between the groups (ifs) or posteriorly (cs, sprs, iprs, and sfs-p). Figure 2*B* visualizes these three clusters on an example cortical surface. The border sulci were substantially deeper and larger than both ventral and dorsal sulci (48.2% and 50.2% deeper on average; 486.2% and 270.7% larger on average; Fig. 4*A*,*B*). Ventral sulci were thicker than both border and dorsal (8.8% and 9.2% thicker on average) and border sulci were similarly thick to dorsal sulci (0.4% thicker on average; Fig. 4*C*). Given the quantitative determination of these three sulcal clusters, subsequent analyses explored whether the morphology of these sulcal clusters changed (1) cross-sectionally between age groups (children ages 6.41-11.53, adolescents ages 11.66-18.86, young adults ages 22-36) and (2) longitudinally in the pediatric sample (ages 6-18 years old). The general clustering of LPFC sulci did not dramatically change when comparing each age group separately (Fig. 3).

LPFC sulcal morphology changes cross-sectionally between children, adolescents, and young adults

To quantify cross-sectional differences in LPFC sulcal morphology between age groups, we first ran a mixed-model ANOVA for each morphologic feature, using within-group factors of hemisphere (left, right) and sulcal cluster (border sulci, dorsal sulci, ventral sulci) and between-group factors of age group (children, adolescents, young adults) and gender (male, female). The main results presented below are with the raw morphologic metrics (for normalized data, see Extended Data Fig. 4-1; for ANOVA tables, see Tables 3-5). Although some features showed gender-related effects, all were nonsignificant when normalized, so we do not report them further (for gender-related effects, see Tables 3-5). Finally, we primarily report age group-related effects here (for hemisphere-related effects, see Tables 3-5).

All morphologic features displayed a main effect of age group except for surface area (Tables 3-5). The depth of LPFC sulci exhibited no differences between adolescents and children ($p > 0.35$, Tukey's adjustment); however, LPFC sulci were deeper in children and adolescents than in young adults (p values < 0.0001, Tukey's adjustment; 11.3% and 9.2% deeper on average, respectively; Fig. 4*A*). There were no age group-related main effects or interactions (with sulcal cluster or hemisphere) for raw surface area (Fig. 4*B*); however, we observed an age group × sulcal cluster effect on normalized surface area (Table 4; Extended Data Fig. 4-1). Conversely, LPFC sulci were thinner in adolescents than in children and young adults (p values < 0.0001, Tukey's adjustment; 6.4% and 6% thinner on average, respectively), but comparable between children and young adults ($p = 0.79$, Tukey's adjustment; Fig. 4*C*). Broadly speaking, then, we observed decreased sulcal depth between the pediatric and young adult age groups and a U-shaped pattern for sulcal thickness (thinnest in adolescence). We also observed age-related differences in normalized (but not raw) surface area that differed by sulcal cluster, with dorsal sulci increasing from adolescence to adulthood, ventral sulci increasing incrementally between childhood and adulthood, and border sulci exhibiting no changes across these age groups.

Considering that there were few differences between children and adolescents as age groups, we followed up these analyses by assessing age continuously using linear mixed-effects models with age and hemisphere in the children and adolescent sample ($N = 72$). These analyses largely confirmed the aforementioned categorical effects: thickness showed significant negative age-related effects, whereas depth and surface area did not (for age-related β and p values, see Fig. 4*D*; Extended Data Fig. 4-1*D*). There were no significant age × hemisphere interactions (p values > 0.06).

Cortical thickness of LPFC sulci changes longitudinally during childhood and adolescence

Considering that sulcal cortical thickness was different in adolescents than children cross-sectionally (Fig. 4*C*), we next specifically

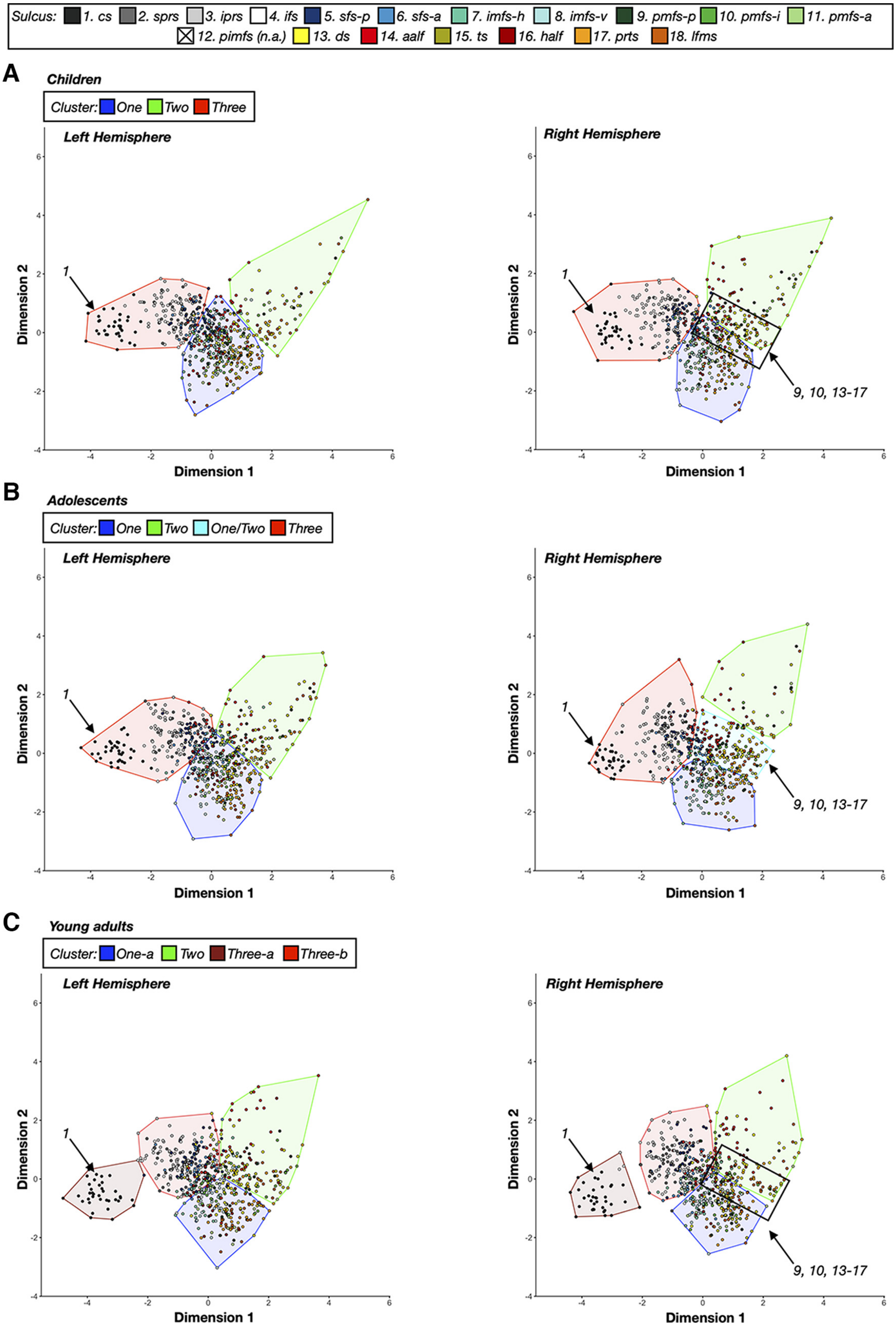

Figure 3. LPFC sulcal clusters for each age group. ***A***, Cluster plots visualizing the results of the *k*-means clustering and multidimensional scaling analysis performed in each hemisphere (left: left hemisphere; right: right hemisphere) for the child sample ($N = 36$). Individual dots represent individual sulci for all 108 participants and are colored by sulcus (see bottom key). Colored ellipses represent the optimal number of clusters that described the LPFC sulci based on morphology (see top key). Black arrows and box represent sulci that split off from the primary cluster in latter plots in ***B*** and ***C***. ***B***, Same as in ***A***, but for the adolescent sample ($N = 36$). ***C***, Same as in ***A***, but for the young adult sample ($N = 36$). For visualization purposes, we reversed the scale on the *x* axis to mirror that of ***A*** and ***B***.

Table 3. Mixed-model ANOVA results for sulcal depth[a]

Effect	DF1	DF2	F	p	Significance	η^2G
Raw (mm)						
age_group	2.000	102.000	24.887	<0.001	***	0.140
gender	1.000	102.000	4.429	0.094	+	0.014
age_group:gender	2.000	102.000	1.406	0.409		0.009
hemi	1.000	102.000	18.632	<0.001	***	0.023
age_group:hemi	2.000	102.000	0.651	0.682		0.002
gender:hemi	1.000	102.000	2.906	0.196		0.004
age_group:gender:hemi	2.000	102.000	0.018	0.982		0.000
age_group:sulcal_cluster	3.500	178.488	2.479	0.127		0.017
gender:sulcal_cluster	1.750	178.488	2.422	0.202		0.008
age_group:gender:sulcal_cluster	3.500	178.488	3.506	0.043	*	0.024
hemi:sulcal_cluster	1.560	159.162	2.806	0.172		0.005
age_group:hemi:sulcal_cluster	3.121	159.162	1.618	0.315		0.006
gender:hemi:sulcal_cluster	1.560	159.162	4.052	0.079	+	0.007
age_group:gender: hemi:sulcal_cluster	3.121	159.162	0.411	0.834		0.002
Normalized (% max depth)						
age_group	2.000	102.000	12.086	<0.001	***	0.083
gender	1.000	102.000	0.544	0.661		0.002
age_group:gender	2.000	102.000	0.136	0.893		0.001
hemi	1.000	102.000	69.367	<0.001	***	0.096
age_group:hemi	2.000	102.000	0.694	0.674		0.002
gender:hemi	1.000	102.000	1.927	0.297		0.003
age_group:gender:hemi	2.000	102.000	0.050	0.962		0.000
age_group:sulcal_cluster	3.455	176.183	2.236	0.172		0.013
gender:sulcal_cluster	1.727	176.183	4.246	0.064	+	0.013
age_group:gender:sulcal_cluster	3.455	176.183	2.956	0.079	+	0.017
hemi:sulcal_cluster	1.562	159.354	3.746	0.092	+	0.006
age_group:hemi:sulcal_cluster	3.125	159.354	1.667	0.301		0.005
gender:hemi:sulcal_cluster	1.562	159.354	3.985	0.081	+	0.006
age_group:gender: hemi:sulcal_cluster	3.125	159.354	0.390	0.834		0.001

[a]Effect size is reported as η^2G. For additional analysis details, see Materials and Methods.
*$p < 0.05$; ***$p < 0.001$; +$p < 0.1$; blank $p \geq 0.01$; FDR-corrected for multiple comparisons.

Table 4. Mixed-model ANOVA results for surface area[a]

Effect	DF1	DF2	F	p	Significance	η^2G
Raw (cm^2)						
age_group	2.000	102.000	1.123	0.52		0.007
gender	1.000	102.000	12.214	0.004	**	0.038
age_group:gender	2.000	102.000	6.757	0.008	**	0.042
hemi	1.000	102.000	2.251	0.251		0.001
age_group:hemi	2.000	102.000	0.778	0.661		0.001
gender:hemi	1.000	102.000	0.061	0.834		0.000
age_group:gender:hemi	2.000	102.000	0.639	0.682		0.001
age_group:sulcal_cluster	2.786	142.105	2.685	0.127		0.023
gender:sulcal_cluster	1.393	142.105	1.436	0.4		0.006
age_group:gender:sulcal_cluster	2.786	142.105	6.988	0.002	**	0.059
hemi:sulcal_cluster	1.470	149.980	0.345	0.747		0.001
age_group:hemi:sulcal_cluster	2.941	149.980	2.221	0.196		0.007
gender:hemi:sulcal_cluster	1.470	149.980	0.558	0.682		0.001
age_group:gender: hemi:sulcal_cluster	2.941	149.980	0.547	0.747		0.002
Normalized (% cortical surface area)						
age_group	2.000	102.000	1.335	0.43		0.004
gender	1.000	102.000	2.162	0.26		0.003
age_group:gender	2.000	102.000	0.929	0.598		0.003
hemi	1.000	102.000	6.273	0.048	*	0.004
age_group:hemi	2.000	102.000	0.886	0.613		0.001
gender:hemi	1.000	102.000	0.082	0.834		0.000
age_group:gender:hemi	2.000	102.000	0.516	0.747		0.001
age_group:sulcal_cluster	3.198	163.101	4.293	0.021	*	0.040
gender:sulcal_cluster	1.599	163.101	4.350	0.064	+	0.021
age_group:gender:sulcal_cluster	3.198	163.101	2.939	0.084	+	0.028
hemi:sulcal_cluster	1.485	151.485	0.144	0.834		0.000
age_group:hemi:sulcal_cluster	2.970	151.485	2.134	0.202		0.012
gender:hemi:sulcal_cluster	1.485	151.485	0.633	0.674		0.002
age_group:gender: hemi:sulcal_cluster	2.970	151.485	0.626	0.747		0.003

[a]Effect size is reported as η^2G. For additional analysis details, see Materials and Methods. Although there was no age group main effect or interactions on raw surface area, there was an age group × sulcal cluster effect on normalized surface area. Here, the normalized surface area of dorsal sulci was smaller in children and adolescents than in young adults (p values ≤ 0.0001, Tukey's adjustment; 11.7% and 11.8% less on average), but comparable between children and adolescents ($p = 0.99$, Tukey's adjustment; Extended Data Fig. 4-1). The normalized surface area of ventral sulci was marginally smaller in children than young adults ($p = 0.067$, Tukey's adjustment) and adolescents ($p = 0.057$, Tukey's adjustment), and comparable between adolescents and young adults ($p = 0.99$, Tukey's adjustment; Extended Data Fig. 4-1). Unlike the dorsal and ventral sulci, no age group differences were observed for border sulci (p values > 0.22, Tukey's adjustment; Extended Data Fig. 4-1).
*$p < 0.05$; **$p < 0.01$; +$p < 0.1$; blank $p \geq 0.01$; FDR-corrected for multiple comparisons.

assessed within-person changes in sulcal cortical thickness during this time period. To this end, we analyzed cortical surfaces for 44 participants in the pediatric sample (6-18 years old) who were scanned at two time points (see Materials and Methods). LPFC sulci were then defined on the base template and projected to the longitudinal reconstruction at the two points, as this procedure provides an accurate sulcal definition at each time point (Fig. 1). We then averaged the cortical thickness of the sulci within each cluster (Fig. 2B) at each time point. Finally, we implemented linear growth curve models to assess whether the cortical thickness of the LPFC sulcal clusters changed from Time point 1 to Time point 2 and whether the baseline age was related to the intercept and the changes.

The cortical thickness of all three LPFC sulcal clusters decreased from Time point 1 to Time point 2, to differing degrees. In both hemispheres, the decrease in cortical thickness was greatest for dorsal sulci (left: β = −0.077, z = −7.26, $p = 3.88\text{e-}13$; right: β = −0.092, z = −5.29, $p = 1.32\text{e-}7$). In the left hemisphere, ventral sulci showed a greater decrease in cortical thickness (β = −0.07, z = −5.08, $p = 3.71\text{e-}7$) than border sulci (β = −0.057, z = −6.31, $p = 2.83\text{e-}10$); in the right hemisphere, on the other hand, ventral sulci showed a comparable decrease (β = −0.051, z = −2.66, $p = 0.0078$) to border sulci (β = −0.053, z = −4.6, $p = 4.23\text{e-}6$). There was no significant variation in the change between participants (p values > 0.22). Further, cortical thickness at Time point 1 (i.e., each individual's intercept) differed as a function of baseline age for all clusters (−0.032 ≤ β values ≤ −0.01, p values < 0.021), such that the older the participant, the lower the starting cortical thickness. However, the change in cortical thickness from Time point 1 to Time point 2 (i.e., the slope) did not differ by baseline age for any cluster in either hemisphere (−0.007 ≤ β values ≤ −0.0001, p values > 0.15). In sum, while all sulcal types showed thinning longitudinally, dorsal sulci showed the most pronounced changes.

Since prior work showed that the average sulcal depth of the frontal lobe declines during adolescence (Alemán-Gómez et al., 2013) and individual differences in sulcal depth are behaviorally significant (Voorhies et al., 2021; Yao et al., 2022), we also tested whether LPFC sulcal depth changed longitudinally, despite the cross-sectional analysis indicating otherwise (Fig. 4A). Indeed, LPFC sulcal depth did not change in our pediatric sample across the average 1.56 year time frame (−0.11 ≤ β values ≤ 0.11, p values > 0.18) and there was no significant variation in the change between participants (p values > 0.13), suggesting that longitudinal changes in LPFC sulcal depth after birth may occur over a longer time span than the one tested here or even after adolescence.

Longitudinal changes in the cortical thickness of LPFC sulci predict developmental changes in matrix reasoning

Given that LPFC sulcal cortical thickness changed across the two time points, we examined whether these changes predicted

Table 5. Mixed-model ANOVA results for cortical thickness[a]

Effect	DF1	DF2	F	p	Significance	η^2G
Raw (mm)						
age_group	2.000	102.000	13.677	<0.001	***	0.100
gender	1.000	102.000	2.452	0.236		0.010
age_group:gender	2.000	102.000	2.114	0.236		0.017
hemi	1.000	102.000	55.734	<0.001	***	0.068
age_group:hemi	2.000	102.000	22.765	<0.001	***	0.056
gender:hemi	1.000	102.000	0.472	0.674		0.001
age_group:gender:hemi	2.000	102.000	0.219	0.834		0.001
age_group:sulcal_cluster	2.993	152.643	3.838	0.042	*	0.020
gender:sulcal_cluster	1.497	152.643	0.920	0.58		0.002
age_group:gender:sulcal_cluster	2.993	152.643	0.566	0.747		0.003
hemi:sulcal_cluster	1.463	149.233	8.365	0.006	**	0.015
age_group:hemi:sulcal_cluster	2.926	149.233	3.377	0.064	+	0.012
gender:hemi:sulcal_cluster	1.463	149.233	0.301	0.757		0.001
age_group:gender: hemi:sulcal_cluster	2.926	149.233	0.571	0.747		0.002
Normalized (% max thickness)						
age_group	2.000	102.000	13.699	<0.001	***	0.100
gender	1.000	102.000	2.469	0.236		0.010
age_group:gender	2.000	102.000	2.121	0.236		0.017
hemi	1.000	102.000	55.899	<0.001	***	0.068
age_group:hemi	2.000	102.000	22.887	<0.001	***	0.056
gender:hemi	1.000	102.000	0.467	0.674		0.001
age_group:gender:hemi	2.000	102.000	0.223	0.834		0.001
age_group:sulcal_cluster	2.988	152.389	3.838	0.042	*	0.020
gender:sulcal_cluster	1.494	152.389	0.908	0.58		0.002
age_group:gender:sulcal_cluster	2.988	152.389	0.566	0.747		0.003
hemi:sulcal_cluster	1.461	149.058	8.411	0.006	**	0.015
age_group:hemi:sulcal_cluster	2.923	149.058	3.366	0.064	+	0.012
gender:hemi:sulcal_cluster	1.461	149.058	0.298	0.757		0.001
age_group:gender: hemi:sulcal_cluster	2.923	149.058	0.565	0.747		0.002

[a]Effect size is reported as η^2G. For additional analysis details, see Materials and Methods.
*$p < 0.05$; **$p < 0.01$; ***$p < 0.001$; +$p < 0.1$; blank $p \geq 0.01$; FDR-corrected for multiple comparisons.

changes in relational reasoning for the 43 participants who completed a matrix reasoning task at two time points. Importantly, participants generally improved from Time point 1 (mean ± SD: 23.3 ± 7.63) to Time point 2 (mean ± SD: 27.2 ± 5.37; $t = -5.01$, $p = 0.00{,}001$, $d = -0.76$, change mean ± SD: 3.9 ± 5.11). In addition, individual variability in ΔCT did not reliably covary with baseline age in either hemisphere [p values > 0.07 (FDR-corrected) for all sulci, except the half (left: $r = 0.26$, $p = 0.042$; right: $r = 0.39$, $p = 0.005$)]. To relate the aforementioned changes in morphology to these changes in cognitive ability, we leveraged a previously published, data-driven pipeline (Voorhies et al., 2021; Yao et al., 2022) to determine which of the LPFC sulci (Table 2), if any, showed a change in cortical thickness (ΔCT) associated with this change in matrix reasoning score (ΔMR). To this end, we implemented a LASSO regression with cross-validation (see Materials and Methods). A LASSO regression not only allows us to select sulci in a data-driven manner but also improves the generalizability of a model and prevents overfitting, especially in situations where there are $10 < x < 25$ predictors (Heinze et al., 2018). We assessed the relationship between ΔCT and ΔMR separately in each hemisphere.

Implementing the LASSO regression revealed that four of the 17 left-hemisphere LPFC sulci in this study were selected at the α value that minimized cross-validated MSE (α = 0.07, MSE = 24.28; Fig. 5A), and thus associated with ΔMR. None of the LPFC sulci in the right hemisphere was selected (α = 0.5, MSE = 26.76). Specifically, the pretriangular sulcus (prts; β = 2.89) and the ascending ramus of the lateral fissure (aalf; β = 14.9) showed positive relationships with ΔMR, whereas the lateral marginal frontal sulcus (lfms; β = −8.43) and the anterior component of the posterior middle frontal sulcus (pmfs-a; β = −1.49) showed negative relationships with ΔMR.

To further examine the relationship between the ΔCT of the selected LPFC sulci and ΔMR, we used the LASSO-derived model to predict ΔMR performance and conducted nested model comparisons to evaluate the fit of this LASSO-derived model (see Materials and Methods). All models were fitted with LOOCV. The LASSO-derived model included the ΔCT of the left-hemisphere prts, aalf, lfms, and pmfs-a as predictors of ΔMR in the LOOCV linear regression. Baseline age was also included as a predictor in the model to assess whether this model outperformed baseline age alone. We found that the LASSO-derived model was associated with ΔMR ($R^2_{CV} = 0.22$, $MSE_{CV} = 19.94$) and showed a moderate relationship between predicted and measured ΔMR (Spearman's $\rho = 0.49$, $p = 0.0008$; Fig. 5B).

Compared with a nested cross-validated model with all 17 LPFC sulci in the left hemisphere in this study and baseline age, we found that the addition of the other 13 sulci greatly weakened the model fit ($R^2_{CV} < 0.01$, $MSE_{CV} = 41.69$; Fig. 5C). This comparison was consistent with the predictions of the LASSO regression. To determine whether the LASSO-derived model explained unique variance in ΔMR relative to baseline age, we compared this model to a nested cross-validated model with baseline age as the sole predictor. Compared with the baseline age model ($R^2_{CV} = 0.098$, $MSE_{CV} = 23.03$; Fig. 5C), the LASSO-derived model showed increased prediction accuracy and decreased MSE_{CV} (Fig. 5C). Thus, the inclusion of the four selected LPFC sulci improved the prediction of ΔMR above and beyond baseline age; however, the addition of the remaining 13 LPFC sulci weakened the fit.

Discussion

To our knowledge, this is the first study to examine how LPFC sulcal morphology changes cross-sectionally and longitudinally, and whether a developmental relationship exists between LPFC sulcal morphology and cognitive performance. This work builds on the rich literature examining how cortical morphology changes during child development (Gogtay et al., 2004; Lebel et al., 2008; Shaw et al., 2008; Alemán-Gómez et al., 2013; Fjell et al., 2015; Amlien et al., 2016; Tamnes et al., 2017; Norbom et al., 2021, 2022; Baum et al., 2022; Bethlehem et al., 2022; Fuhrmann et al., 2022) and how LPFC maturation is linked to reasoning performance (Crone et al., 2009; Dumontheil et al., 2010; Wendelken et al., 2017; Leonard et al., 2019). Importantly, these findings reveal, at a more granular level, yet another way in which PFC is linked to reasoning performance (Milner and Petrides, 1984; Christoff et al., 2001; Vendetti and Bunge, 2014; Aichelburg et al., 2016; Urbanski et al., 2016; Hartogsveld et al., 2018; Assem et al., 2020; Holyoak and Monti, 2021). Leveraging one of the largest samplings of LPFC sulci within individual participants, we observed a striking complexity in how the morphology of a single cortical region changes. Further, our results show that longitudinal morphologic changes in four left-hemisphere LPFC sulci are cognitively relevant during middle childhood and adolescence.

On the development of sulcal morphology

We found that some, but not all, morphologic features of LPFC sulci differ cross-sectionally between age groups and change longitudinally in children and adolescents. Specifically, while most morphologic features differed between children/adolescents and young

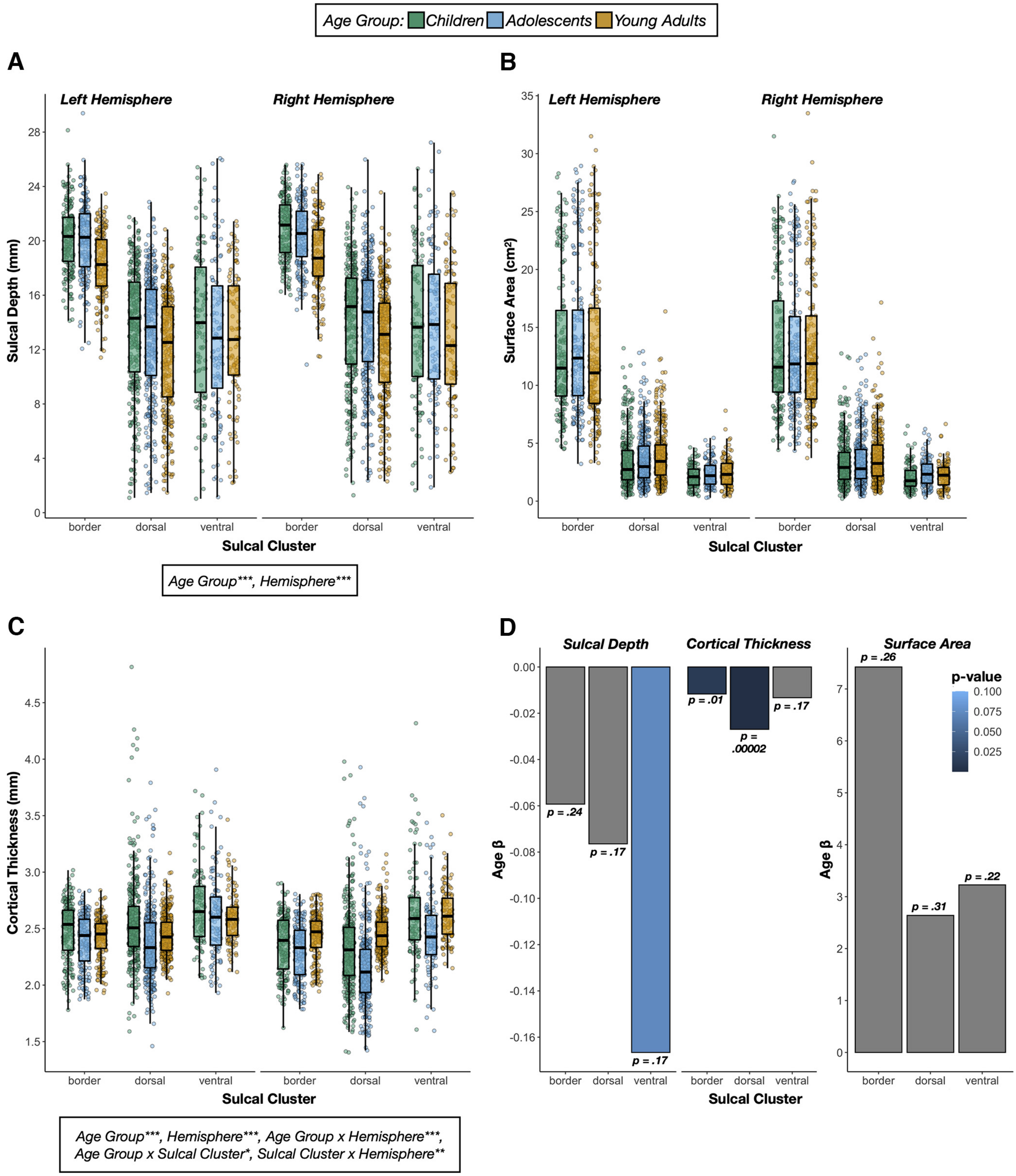

Figure 4. Some, but not all, morphologic features of LPFC sulci differ between age groups cross-sectionally. ***A***, Boxplot visualizing sulcal depth (mm) as a function of sulcal cluster (*x* axis), age group (green represents children; blue represents adolescents; yellow represents young adults; $N = 36$ each), and hemisphere (left vs right faceted plot). Individual dots represent each participant's individual sulci in each cluster as described in Figure 2*B*. The legend under the plot displays the significant results (i.e., related to age group, hemisphere, and sulcal cluster) from the mixed-model ANOVAs shown in Tables 3-5. $*p < 0.05$. $**p < 0.01$. $***p < 0.001$. For gender-related effects, see Tables 3-5. ***B***, Same as in ***A***, but for surface area (cm^2). ***C***, Same as in ***A***, but for mean cortical thickness (mm). ***D***, Results of the linear mixed effects models treating age as a continuous variable in the children and adolescent sample ($N = 72$). Bars represent the β-coefficients for the effect of age on each raw metric. Each bar is colored by the *p* value for the β it indicates. Gray bars represent $p > 0.10$. Because of the large difference in scale, surface area has a separate *y* axis. For normalized data, see Extended Data Figure 4-1.

 J. Neurosci., April 5, 2023 • 43(14):2552–2567

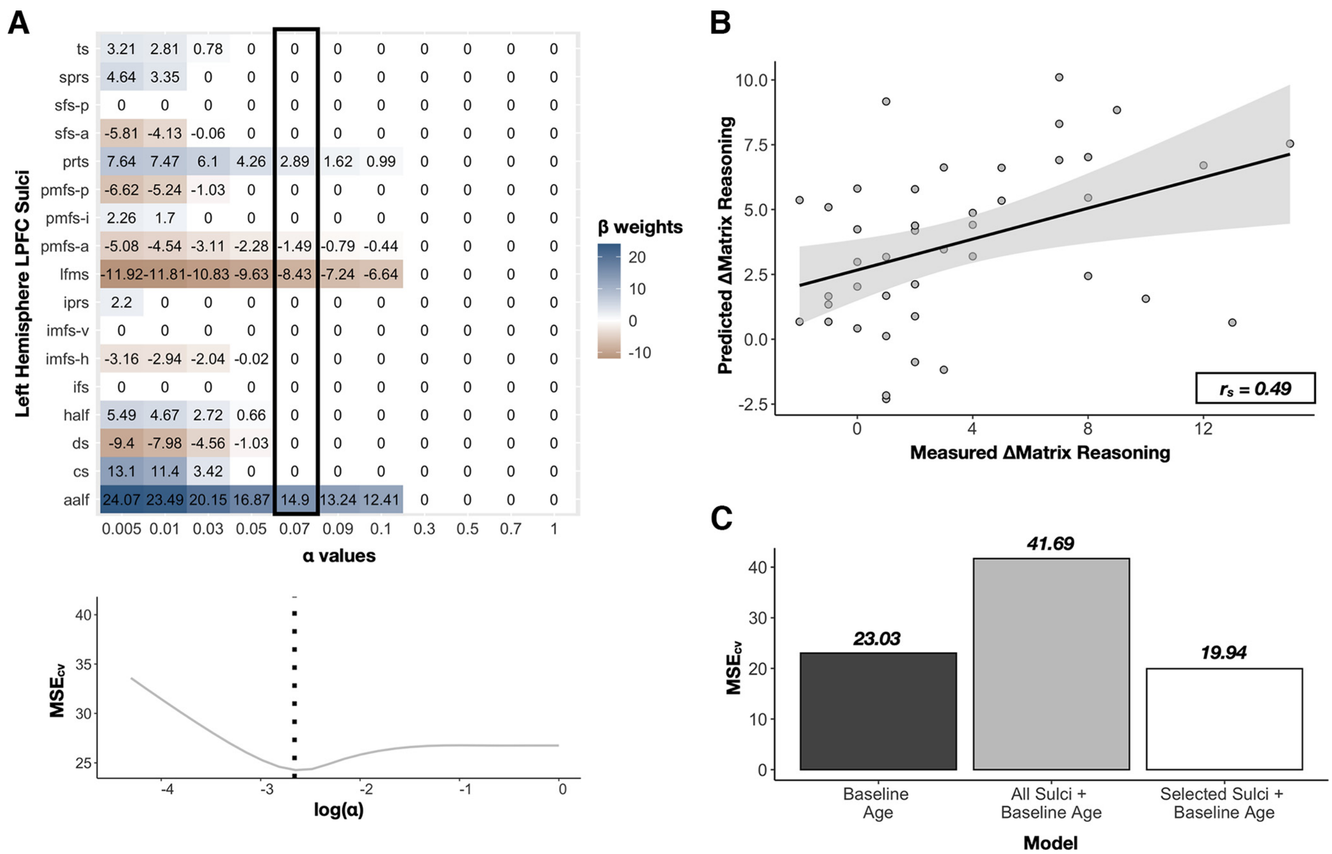

Figure 5. Data-driven model selection reveals that longitudinal changes in cortical thickness of LPFC sulci are associated with longitudinal changes in reasoning performance. Performance and model fits relating change in sulcal cortical thickness (ΔCT) to change in reasoning performance (ΔMR). ***A***, Top, β-coefficients for each sulcus across a range of shrinking parameter (α) values resulting from the LASSO regression in the left hemisphere. Highlighted box represents the coefficients at the chosen α level with the lowest MSE_{cv}. Bottom, MSE_{cv} at each α level. We selected the α value that minimized MSE_{cv} (dotted black line). The LASSO regression with right-hemisphere LPFC sulci selected no sulci at the α value that minimized MSE_{cv}. ***B***, Spearman's correlation ($r_s = 0.49$) between participants' measured ΔMR scores and the predicted ΔMR scores from the LOOCV linear regression for the selected model in ***A***, which had four left-hemisphere LPFC sulci and baseline age as predictors. ***C***, Model comparison of the cross-validated MSEs of a model with baseline age as its only predictor (black), a model with all left-hemisphere LPFC sulci and baseline age as predictors (gray), and a model with the four selected left hemisphere sulci and baseline age as predictors (white). The model with left-hemisphere sulci selected by the LASSO regression (white) had the lowest MSE_{cv}, thus performing the best. Strikingly, the four selected left hemisphere sulci coincide with meta-analysis activation maps for reasoning made with Neurosynth (see Fig. 6).

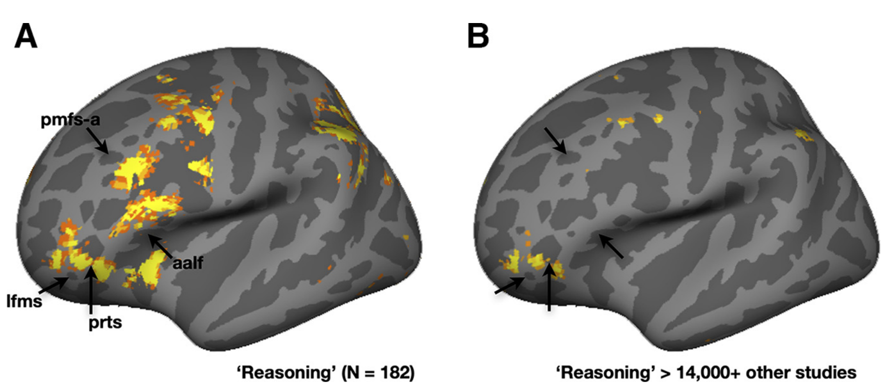

Figure 6. Selected LPFC sulci colocalize with functional activation for reasoning-related key words in a meta-analysis using NeuroSynth. ***A***. Left hemisphere inflated *fsaverage* cortical surface displaying overlap visualization of a whole-brain FDR-corrected ($p < 0.01$) uniformity-test meta-analysis *z* score map of the "reasoning" term (downloaded from Neurosynth; https://neurosynth.org/). This map was generated from a χ^2 test comparing the activation in each voxel for studies containing the term ($N = 182$) compared with what one would expect if activation were uniformly distributed throughout the gray matter. The four left-hemisphere LPFC sulci selected by the LASSO regression are identified on this surface with black arrows. ***B***, Same as in ***A***, but instead displaying overlap visualization of a whole-brain FDR-corrected ($p < 0.01$) association-test meta-analysis *z* score map of the "reasoning" term. This map was generated from a χ^2 test comparing the proportion of studies demonstrating activation in each voxel for studies containing the term ($N = 182$) of interest compared with all other studies in the database ($N > 14,000$).

adults, only cortical thickness showed cross-sectional differences between children and adolescents and longitudinal changes during this time frame (6-18 years). These age-related differences were not homogeneous across our data-driven sulcal clusters or between cerebral hemispheres. This complexity suggests that a more nuanced approach is necessary to understand cortical development. As the field of neuroscience debates the importance of, and differences between, "large N" and "deep imaging" approaches (Genon et al., 2022; Gratton et al., 2022), our results and prior work (Raznahan et al., 2011; Alemán-Gómez et al., 2013; Cachia et al., 2016; Bethlehem et al., 2022; Fuhrmann et al., 2022) emphasize that deep imaging analyses are crucial for delineating how, when, and where changes in cortical morphology occur during development.

Additionally, the lack of effects regarding some morphologic features (notably depth and surface area) during childhood and adolescence does not imply that these features do not change during development, as documented in prior work at the lobular level (Alemán-Gómez et al., 2013). With regard to longitudinal results, we may not see sublobular morphologic differences across this age range if changes take place over a longer period than measured here (on average, 1.56 years between time points). Indeed, our results presented cross-sectional differences in most features between children/adolescents and young adults, suggesting that the delay between longitudinal time points may have been too brief. With regard to cross-sectional results, it may be that the most pronounced changes in LPFC sulcal morphology occur outside of the 6-18 age range: in particular, during the prenatal period and early childhood (Dubois et al., 2008; Meng et al., 2014; Le Guen et al., 2018; Im and Grant, 2019; Aslan Çetin and Madazlı, 2021), and again in older adulthood (Rettmann, 2005; Liu et al., 2013; Madan, 2019, 2021; Tang et al., 2021; Willbrand et al., 2022a).

On the relationship between LPFC and reasoning

Using a data-driven approach, we found that changes in gray matter thickness of four left-hemisphere LPFC sulci predicted changes in reasoning performance. Strikingly, two of the four selected sulci, lfms and prts, likely border or fall within rostrolateral PFC, a subregion of LPFC implicated in reasoning based on neuropsychological and fMRI data (Milner and Petrides, 1984; Christoff et al., 2001; Vendetti and Bunge, 2014; Aichelburg et al., 2016; Urbanski et al., 2016; Hartogsveld et al., 2018; Assem et al., 2020; Holyoak and Monti, 2021). Indeed, these two sulci colocalize with activation strongly linked to reasoning in a meta-analysis comparing 182 fMRI studies including this term with >14,000 studies that did not include this term (via *Neurosynth*; Fig. 6). The other two implicated sulci, pmfs-a and aalf, likely border dorsolateral and ventrolateral PFC regions that were also implicated in reasoning in the fMRI meta-analysis; of these, the pmfs-a was linked more closely to reasoning than to other cognitive processes.

Building on prior work linking subdivisions of LPFC to reasoning, our results suggest four small individually identified sulci that may serve as personalized "coordinates" of a larger cognitive globe (Stuss and Benson, 1984; Miller et al., 2021a). By integrating these and previous findings, future studies can work toward building a multimodal understanding across spatial scales regarding the neuroanatomical substrates of reasoning within and beyond LPFC subregions, both involving the current dataset (Wendelken et al., 2017; Voorhies et al., 2021; Willbrand et al., 2022b) and others (e.g., Ritchie et al., 2015; Chen et al., 2020). Other factors to consider are that anatomic relations to reasoning can vary over time (Shaw et al., 2006), and can depend on the population under consideration, with children from higher and lower socioeconomic backgrounds exhibiting different trajectories of cortical thinning during childhood (Piccolo et al., 2016) and different relations between cortical thickness and reasoning (Leonard et al., 2019).

On relationships between sulcal morphology and human behavior

Sanides (1964) proposed a classic theory linking tertiary sulci, the last sulci to emerge in gestation, to later-developing cognitive abilities supported by association cortices. Focusing on LPFC, he proposed that the late emergence and continued postnatal morphologic development of tertiary sulci are likely related to the cognitive skills associated with LPFC, which also show protracted development (Sanides, 1964). Our findings provide the first empirical support for a longitudinal aspect of this theory by showing that one such feature of specific LPFC tertiary sulci (gray matter thickness) is predictive of the development of one such ability (reasoning).

These findings also build on prior research identifying that the trajectory of change in cortical thickness, not necessarily the thickness itself, is linked to reasoning (Shaw et al., 2006; Burgaleta et al., 2014; Schnack et al., 2015). However, these studies did not consider the cortex buried within specific cortical folds across individuals. Thus, this study extends this relationship to specific areas of cortex buried in LPFC sulci. Mechanistically, cortical thinning likely reflects not only gray matter thinning but also the myelination of fibers extending into the cortical ribbon (Paus, 2005; de Faria et al., 2021; Norbom et al., 2021; Baum et al., 2022). Indeed, recent work by Natu et al. (2019) found that myelination is a key contributor to cortical thinning in the visual cortex during childhood. Therefore, changes in sulcal cortical thickness may reflect changes in the local cellular architecture and neural circuits that ultimately support the development of reasoning abilities during childhood and adolescence, a relationship that should be explored in future research.

Our findings also extend prior research on the relationship between sulcal morphology and behavior from cross-sectional individual differences to longitudinal changes within participants. For example, recent work has found that individual differences in sulcal depth, especially in LPFC, are predictive of individual differences in cognitive tasks during childhood and adolescence, more so than individual differences in sulcal thickness (Voorhies et al., 2021; Yao et al., 2022). However, as mentioned earlier in this Discussion, our findings and previous work (Shaw et al., 2006; Burgaleta et al., 2014; Schnack et al., 2015) emphasize that it is the trajectory of thinning that is cognitively meaningful and that depth does not appear to change during childhood and adolescence, both cross-sectionally and longitudinally. Nevertheless, sulcal depth could change over a longer period of time and a different time frame than what was studied here. Accordingly, future research should discern whether depth changes do occur in these sulci over a longer longitudinal period of time during middle childhood and adolescence and, if so, determine whether these changes are cognitively relevant.

Future directions

The present findings were primarily limited by the number of time points and the brief time interval between them, as well as the limited age ranges, either or both of which could have precluded detection of nuanced morphologic changes (e.g., with sulcal depth and surface area). Further, we did not assess all possible morphologic features (e.g., sulcal width and length) because of methodological limitations of the analysis software (see Materials and Methods). Future work should assess changes in all possible morphologic features at the level of individual sulci, across numerous time points, spanning early development through older adulthood. Such an extension could reveal additional developmental changes and relations to behavior. In closing, these results relay the importance of considering individual differences in neuroanatomy when studying the neurodevelopment of the cerebral cortex. In so doing, they lay the foundation for more precise developmental, structural-functional, and structural-behavioral analyses that help to elucidate how brain anatomy and its development supports emerging cognitive functions.

References

Aichelburg C, Urbanski M, Thiebaut de Schotten M, Humbert F, Levy R, Volle E (2016) Morphometry of left frontal and temporal poles predicts analogical reasoning abilities. Cereb Cortex 26:915–932.

Alemán-Gómez Y, Janssen J, Schnack H, Balaban E, Pina-Camacho L, Alfaro-Almagro F, Castro-Fornieles J, Otero S, Baeza I, Moreno D, Bargalló N, Parellada M, Arango C, Desco M (2013) The human cerebral cortex flattens during adolescence. J Neurosci 33:15004–15010.

Amiez C, Petrides M (2007) Selective involvement of the mid-dorsolateral prefrontal cortex in the coding of the serial order of visual stimuli in working memory. Proc Natl Acad Sci USA 104:13786–13791.

Amlien IK, Fjell AM, Tamnes CK, Grydeland H, Krogsrud SK, Chaplin TA, Rosa MG, Walhovd KB (2016) Organizing principles of human cortical development–thickness and area from 4 to 30 years: insights from comparative primate neuroanatomy. Cereb Cortex 26:257–267.

Armstrong E, Schleicher A, Omran H, Curtis M, Zilles K (1995) The ontogeny of human gyrification. Cereb Cortex 5:56–63.

Aslan Çetin B, Madazlı R (2021) Assessment of normal fetal cortical sulcus development. Arch Gynecol Obstet 306:735–743.

Assem M, Glasser MF, Van Essen DC, Duncan J (2020) A domain-general cognitive core defined in multimodally parcellated human cortex. Cereb Cortex 30:4361–4380.

Baum GL, Flournoy JC, Glasser MF, Harms MP, Mair P, Sanders AF, Barch DM, Buckner RL, Bookheimer S, Dapretto M, Smith S, Thomas KM, Yacoub E, Van Essen DC, Somerville LH (2022) Graded variation in T1w/T2w ratio during adolescence: measurement, caveats, and implications for development of cortical myelin. J Neurosci 42:5681–5694.

Bethlehem RAI, et al., VETSA (2022) Brain charts for the human lifespan. Nature 604:525–533.

Borne L, Rivière D, Mancip M, Mangin JF (2020) Automatic labeling of cortical sulci using patch- or CNN-based segmentation techniques combined with bottom-up geometric constraints. Med Image Anal 62:101651.

Brown TT, et al. (2012) Neuroanatomical assessment of biological maturity. Curr Biol 22:1693–1698.

Burgaleta M, Johnson W, Waber DP, Colom R, Karama S (2014) Cognitive ability changes and dynamics of cortical thickness development in healthy children and adolescents. Neuroimage 84:810–819.

Cachia A, Borst G, Tissier C, Fisher C, Plaze M, Gay O, Rivière D, Gogtay N, Giedd J, Mangin JF, Houdé O, Raznahan A (2016) Longitudinal stability of the folding pattern of the anterior cingulate cortex during development. Dev Cogn Neurosci 19:122–127.

Cao B, Mwangi B, Passos IC, Wu MJ, Keser Z, Zunta-Soares GB, Xu D, Hasan KM, Soares JC (2017) Lifespan gyrification trajectories of human brain in healthy individuals and patients with major psychiatric disorders. Sci Rep 7:511.

Carmona S, et al. (2019) Pregnancy and adolescence entail similar neuroanatomical adaptations: a comparative analysis of cerebral morphometric changes. Hum Brain Mapp 40:2143–2152.

Charrad M, Ghazzali N, Boiteau V, Niknafs A (2014) NbClust: an R package for determining the relevant number of clusters in a data set. J Stat Softw 61:1–36.

Chen PY, Chen CL, Hsu YC, Tseng WY, Cam-CAN (2020) Fluid intelligence is associated with cortical volume and white matter tract integrity within multiple-demand system across adult lifespan. Neuroimage 212:116576.

Chi JG, Dooling EC, Gilles FH (1977) Gyral development of the human brain. Ann Neurol 1:86–93.

Chini M, Hanganu-Opatz IL (2021) Prefrontal cortex development in health and disease: lessons from rodents and humans. Trends Neurosci 44:227–240.

Christoff K, Prabhakaran V, Dorfman J, Zhao Z, Kroger JK, Holyoak KJ, Gabrieli JD (2001) Rostrolateral prefrontal cortex involvement in relational integration during reasoning. Neuroimage 14:1136–1149.

Crone EA, Wendelken C, van Leijenhorst L, Honomichl RD, Christoff K, Bunge SA (2009) Neurocognitive development of relational reasoning. Dev Sci 12:55–66.

Dale AM, Fischl B, Sereno MI (1999) Cortical surface-based analysis: I. Segmentation and surface reconstruction. Neuroimage 9:179–194.

de Faria O Jr, Pivonkova H, Varga B, Timmler S, Evans KA, Káradóttir RT (2021) Periods of synchronized myelin changes shape brain function and plasticity. Nat Neurosci 24:1508–1521.

Donahue CJ, Glasser MF, Preuss TM, Rilling JK, Van Essen DC (2018) Quantitative assessment of prefrontal cortex in humans relative to nonhuman primates. Proc Natl Acad Sci USA 115:E5183–E5192.

Dubois J, Benders M, Borradori-Tolsa C, Cachia A, Lazeyras F, Ha-Vinh Leuchter R, Sizonenko SV, Warfield SK, Mangin JF, Hüppi PS (2008) Primary cortical folding in the human newborn: an early marker of later functional development. Brain 131:2028–2041.

Dumontheil I, Houlton R, Christoff K, Blakemore SJ (2010) Development of relational reasoning during adolescence. Dev Sci 13:F15–F24.

Ferrer E, Whitaker KJ, Steele JS, Green CT, Wendelken C, Bunge SA (2013) White matter maturation supports the development of reasoning ability through its influence on processing speed. Dev Sci 16:941–951.

Fischl B, Dale AM (2000) Measuring the thickness of the human cerebral cortex from magnetic resonance images. Proc Natl Acad Sci USA 97:11050–11055.

Fischl B, Sereno MI, Dale AM (1999a) Cortical surface-based analysis: II. Inflation, flattening, and a surface-based coordinate system. Neuroimage 9:195–207.

Fischl B, Sereno MI, Tootell RB, Dale AM (1999b) High-resolution intersubject averaging and a coordinate system for the cortical surface. Hum Brain Mapp 8:272–284.

Fjell AM, et al. (2015) Development and aging of cortical thickness correspond to genetic organization patterns. Proc Natl Acad Sci USA 112:15462–15467.

Fuhrmann D, Madsen KS, Johansen LB, Baaré WF, Kievit RA (2022) The midpoint of cortical thinning between late childhood and early adulthood differs between individuals and brain regions: evidence from longitudinal modelling in a 12-wave neuroimaging sample. Neuroimage 261:119507.

Genon S, Eickhoff SB, Kharabian S (2022) Linking interindividual variability in brain structure to behaviour. Nat Rev Neurosci 23:307–318.

Ghojogh B, Crowley M (2019) The theory behind overfitting, cross validation, regularization, bagging, and boosting: tutorial. arXiv.

Glasser MF, Sotiropoulos SN, Wilson JA, Coalson TS, Fischl B, Andersson JL, Xu J, Jbabdi S, Webster M, Polimeni JR, Van Essen DC, Jenkinson M, WU-Minn HCP Consortium (2013) The minimal preprocessing pipelines for the Human Connectome Project. Neuroimage 80:105–124.

Gogtay N, Giedd JN, Lusk L, Hayashi KM, Greenstein D, Vaituzis AC, Nugent TF 3rd, Herman DH, Clasen LS, Toga AW, Rapoport JL, Thompson PM (2004) Dynamic mapping of human cortical development during childhood through early adulthood. Proc Natl Acad Sci USA 101:8174–8179.

Gottfredson LS (1997) Why g matters: the complexity of everyday life. Intelligence 24:79–132.

Gratton C, Nelson SM, Gordon EM (2022) Brain-behavior correlations: two paths toward reliability. Neuron 110:1446–1449.

Hartogsveld B, Bramson B, Vijayakumar S, van Campen AD, Marques JP, Roelofs K, Toni I, Bekkering H, Mars RB (2018) Lateral frontal pole and relational processing: activation patterns and connectivity profile. Behav Brain Res 355:2–11.

Hathaway CB, Voorhies WI, Sathishkumar N, Mittal C, Yao JK, Miller JA, Parker BJ, Weiner KS (2022) Defining tertiary sulci in lateral prefrontal cortex in chimpanzees using human predictions. bioRxiv 2022.04.12.488091.

Heinze G, Wallisch C, Dunkler D (2018) Variable selection: a review and recommendations for the practicing statistician. Biom J 60:431–449.

Holyoak KJ, Monti MM (2021) Relational integration in the human brain: a review and synthesis. J Cogn Neurosci 33:341–356.

Im K, Grant PE (2019) Sulcal pits and patterns in developing human brains. Neuroimage 185:881–890.

Jin K, Zhang T, Shaw M, Sachdev P, Cherbuin N (2018) Relationship between sulcal characteristics and brain aging. Front Aging Neurosci 10:339.

Krawczyk DC (2012) The cognition and neuroscience of relational reasoning. Brain Res 1428:13–23.

Le Guen Y, Auzias G, Leroy F, Noulhiane M, Dehaene-Lambertz G, Duchesnay E, Mangin JF, Coulon O, Frouin V (2018) Genetic influence on the sulcal pits: on the origin of the first cortical folds. Cereb Cortex 28:1922–1933.

Lebel C, Walker L, Leemans A, Phillips L, Beaulieu C (2008) Microstructural maturation of the human brain from childhood to adulthood. Neuroimage 40:1044–1055.

Leonard JA, Romeo RR, Park AT, Takada ME, Robinson ST, Grotzinger H, Last BS, Finn AS, Gabrieli JD, Mackey AP (2019) Associations between cortical thickness and reasoning differ by socioeconomic status in development. Dev Cogn Neurosci 36:100641.

Li X, Zhang S, Jiang X, Zhang S, Han J, Guo L, Zhang T (2022) Cortical development coupling between surface area and sulcal depth on macaque brains. Brain Struct Funct 227:1013–1029.

Liu T, Sachdev PS, Lipnicki DM, Jiang J, Cui Y, Kochan NA, Reppermund S, Trollor JN, Brodaty H, Wen W (2013) Longitudinal changes in sulcal morphology associated with late-life aging and MCI. Neuroimage 74:337–342.

Lopez-Persem A, Verhagen L, Amiez C, Petrides M, Sallet J (2019) The human ventromedial prefrontal cortex: sulcal morphology and its influence on functional organization. J Neurosci 39:3627–3639.

Luria AR (1966) Higher cortical functions in man. New York: Springer.

Madan CR (2019) Robust estimation of sulcal morphology. Brain Inform 6:5.

Madan CR (2021) Age-related decrements in cortical gyrification: evidence from an accelerated longitudinal dataset. Eur J Neurosci 53:1661–1671.

Meng Y, Li G, Lin W, Gilmore JH, Shen D (2014) Spatial distribution and longitudinal development of deep cortical sulcal landmarks in infants. Neuroimage 100:206–218.

Miller JA, Voorhies WI, Li X, Raghuram I, Palomero-Gallagher N, Zilles K, Sherwood CC, Hopkins WD, Weiner KS (2020) Sulcal morphology of ventral temporal cortex is shared between humans and other hominoids. Sci Rep 10:17132.

Miller JA, D'Esposito M, Weiner KS (2021a) Using tertiary sulci to map the 'cognitive globe' of prefrontal cortex. J Cogn Neurosci 33:1698–1715.

Miller JA, Voorhies WI, Lurie DJ, D'Esposito M, Weiner KS (2021b) Overlooked tertiary sulci serve as a meso-scale link between microstructural and functional properties of human lateral prefrontal cortex. J Neurosci 41:2229–2244.

Milner B, Petrides M (1984) Behavioural effects of frontal-lobe lesions in man. Trends Neurosci 7:403–407.

Natu VS, Gomez J, Barnett M, Jeska B, Kirilina E, Jaeger C, Zhen Z, Cox S, Weiner KS, Weiskopf N, Grill-Spector K (2019) Apparent thinning of human visual cortex during childhood is associated with myelination. Proc Natl Acad Sci USA 116:20750–20759.

Natu VS, Arcaro MJ, Barnett MA, Gomez J, Livingstone M, Grill-Spector K, Weiner KS (2021) Sulcal depth in the medial ventral temporal cortex predicts the location of a place-selective region in macaques, children, and adults. Cereb Cortex 31:48–61.

Norbom LB, Ferschmann L, Parker N, Agartz I, Andreassen OA, Paus T, Westlye LT, Tamnes CK (2021) New insights into the dynamic development of the cerebral cortex in childhood and adolescence: integrating macro- and microstructural MRI findings. Prog Neurobiol 204:102109.

Norbom LB, Hanson J, van der Meer D, Ferschmann L, Røysamb E, von Soest T, Andreassen OA, Agartz I, Westlye LT, Tamnes CK (2022) Parental socioeconomic status is linked to cortical microstructure and language abilities in children and adolescents. Dev Cogn Neurosci 56:101132.

Paus T (2005) Mapping brain maturation and cognitive development during adolescence. Trends Cogn Sci 9:60–68.

Pedregosa F, Varoquaux G, Gramfort A, Michel V, Thirion B, Grisel O, Blondel M, Prettenhofer P, Weiss R, Dubourg V, Vanderplas J, Passos A, Cournapeau D, Brucher M, Perrot M, Duchesnay E (2011) Scikit-learn: machine learning in Python. J Machine 12:2825–2830.

Petrides M (2019) Atlas of the morphology of the human cerebral cortex on the average MNI brain. San Diego: Academic.

Piccolo LR, Merz EC, He X, Sowell ER, Noble KG, Pediatric Imaging, Neurocognition, Genetics Study (2016) Age-related differences in cortical thickness vary by socioeconomic status. PLoS One 11:e0162511.

Raznahan A, Shaw P, Lalonde F, Stockman M, Wallace GL, Greenstein D, Clasen L, Gogtay N, Giedd JN (2011) How does your cortex grow? J Neurosci 31:7174–7177.

Rettmann ME (2005) Cross-sectional and longitudinal analyses of anatomical sulcal changes associated with aging. Cereb Cortex 16:1584–1594.

Reuter M, Fischl B (2011) Avoiding asymmetry-induced bias in longitudinal image processing. Neuroimage 57:19–21.

Reuter M, Rosas HD, Fischl B (2010) Highly accurate inverse consistent registration: a robust approach. Neuroimage 53:1181–1196.

Reuter M, Schmansky NJ, Rosas HD, Fischl B (2012) Within-subject template estimation for unbiased longitudinal image analysis. Neuroimage 61:1402–1418.

Ritchie SJ, Booth T, Valdés Hernández MD, Corley J, Maniega SM, Gow AJ, Royle NA, Pattie A, Karama S, Starr JM, Bastin ME, Wardlaw JM, Deary IJ (2015) Beyond a bigger brain: multivariable structural brain imaging and intelligence. Intelligence 51:47–56.

Sanides F (1964) Structure and function of the human frontal lobe. Neuropsychologia 2:209–219.

Schaer M, Cuadra MB, Tamarit L, Lazeyras F, Eliez S, Thiran J-P (2008) A surface-based approach to quantify local cortical gyrification. IEEE Trans Med Imaging 27:161–170.

Schaer M, Cuadra MB, Schmansky N, Fischl B, Thiran JP, Eliez S (2012) How to measure cortical folding from MR images: a step-by-step tutorial to compute local gyrification index. J Vis Exp 59:e3417.

Schnack HG, van Haren NE, Brouwer RM, Evans A, Durston S, Boomsma DI, Kahn RS, Hulshoff Pol HE (2015) Changes in thickness and surface area of the human cortex and their relationship with intelligence. Cereb Cortex 25:1608–1617.

Semendeferi K, Lu A, Schenker N, Damasio H (2002) Humans and great apes share a large frontal cortex. Nat Neurosci 5:272–276.

Shaw P, Greenstein D, Lerch J, Clasen L, Lenroot R, Gogtay N, Evans A, Rapoport J, Giedd J (2006) Intellectual ability and cortical development in children and adolescents. Nature 440:676–679.

Shaw P, Kabani NJ, Lerch JP, Eckstrand K, Lenroot R, Gogtay N, Greenstein D, Clasen L, Evans A, Rapoport JL, Giedd JN, Wise SP (2008) Neurodevelopmental trajectories of the human cerebral cortex. J Neurosci 28:3586–3594.

Sowell ER, Thompson PM, Leonard CM, Welcome SE, Kan E, Toga AW (2004) Longitudinal mapping of cortical thickness and brain growth in normal children. J Neurosci 24:8223–8231.

Sprung-Much T, Petrides M (2018) Morphological patterns and spatial probability maps of two defining sulci of the posterior ventrolateral frontal cortex of the human brain: the sulcus diagonalis and the anterior ascending ramus of the lateral fissure. Brain Struct Funct 223:4125–4152.

Sprung-Much T, Petrides M (2020) Morphology and spatial probability maps of the horizontal ascending ramus of the lateral fissure. Cereb Cortex 30:1586–1602.

Stuss DT, Benson DF (1984) Neuropsychological studies of the frontal lobes. Psychol Bull 95:3–28.

Stuss DT, Knight RT (2013) Principles of frontal lobe function. New York: Oxford UP.

Tamnes CK, Walhovd KB, Dale AM, Østby Y, Grydeland H, Richardson G, Westlye LT, Roddey JC, Hagler DJ Jr, Due-Tønnessen P, Holland D, Fjell AM, Alzheimer's Disease Neuroimaging Initiative (2013) Brain development and aging: overlapping and unique patterns of change. Neuroimage 68:63–74.

Tamnes CK, Herting MM, Goddings AL, Meuwese R, Blakemore SJ, Dahl RE, Güroğlu B, Raznahan A, Sowell ER, Crone EA, Mills KL (2017) Development of the cerebral cortex across adolescence: a multisample study of inter-related longitudinal changes in cortical volume, surface area, and thickness. J Neurosci 37:3402–3412.

Tang H, Liu T, Liu H, Jiang J, Cheng J, Niu H, Li S, Brodaty H, Sachdev P, Wen W (2021) A slower rate of sulcal widening in the brains of the nondemented oldest old. Neuroimage 229:117740.

Urbanski M, Bréchemier ML, Garcin B, Bendetowicz D, Thiebaut de Schotten M, Foulon C, Rosso C, Clarençon F, Dupont S, Pradat-Diehl P, Labeyrie MA, Levy R, Volle E (2016) Reasoning by analogy requires the left frontal pole: lesion-deficit mapping and clinical implications. Brain 139:1783–1799.

Van Essen DC, et al. (2012) The Human Connectome Project: a data acquisition perspective. Neuroimage 62:2222–2231.

Vendetti MS, Bunge SA (2014) Evolutionary and developmental changes in the lateral frontoparietal network: a little goes a long way for higher-level cognition. Neuron 84:906–917.

Voorhies WI, Miller JA, Yao JK, Bunge SA, Weiner KS (2021) Cognitive insights from tertiary sulci in prefrontal cortex. Nat Commun 12:5122.

Wechsler D (1949) Wechsler Intelligence Scale for Children; manual. https://psycnet.apa.org/fulltext/1950-00877-000.pdf.

Weiner KS (2019) The mid-fusiform sulcus (sulcus sagittalis gyri fusiformis). Anat Rec (Hoboken) 302:1491–1503.

Weiner KS, Golarai G, Caspers J, Chuapoco MR, Mohlberg H, Zilles K, Amunts K, Grill-Spector K (2014) The mid-fusiform sulcus: a landmark identifying both cytoarchitectonic and functional divisions of human ventral temporal cortex. Neuroimage 84:453–465.

Weiner KS, Natu VS, Grill-Spector K (2018) On object selectivity and the anatomy of the human fusiform gyrus. Neuroimage 173:604–609.

Welker W (1990) Why does cerebral cortex fissure and fold? In: Cerebral cortex: comparative structure and evolution of cerebral cortex (Jones EG, Peters A, eds), Vol II, pp 3–136. New York: Springer.

Wendelken C, O'Hare ED, Whitaker KJ, Ferrer E, Bunge SA (2011) Increased functional selectivity over development in rostrolateral prefrontal cortex. J Neurosci 31:17260–17268.

Wendelken C, Ferrer E, Whitaker KJ, Bunge SA (2016) Fronto-parietal network reconfiguration supports the development of reasoning ability. Cereb Cortex 26:2178–2190.

Wendelken C, Ferrer E, Ghetti S, Bailey SK, Cutting L, Bunge SA (2017) Frontoparietal structural connectivity in childhood predicts development of functional connectivity and reasoning ability: a large-scale longitudinal investigation. J Neurosci 37:8549–8558.

Willbrand EH, Parker BJ, Voorhies WI, Miller JA, Lyu I, Hallock T, Aponik-Gremillion L, Koslov SR, Null N, Bunge SA, Foster BL, Weiner KS (2022a) Uncovering a tripartite landmark in posterior cingulate cortex. Sci Adv 8:eabn9516.

Willbrand EH, Voorhies WI, Yao JK, Weiner KS, Bunge SA (2022b) Presence or absence of a prefrontal sulcus is linked to reasoning performance during child development. Brain Struct Funct 227:2543–2551.

Yao JK, Voorhies WI, Miller JA, Bunge SA, Weiner KS (2022) Sulcal depth in prefrontal cortex: a novel predictor of working memory performance. Cereb Cortex bhac173.

Zhou Q, Goryawala M, Cabrerizo M, Barker W, Duara R, Adjouadi M (2014) Significance of normalization on anatomical MRI measures in predicting Alzheimer's disease. Sci World J 2014:541802.